Mon. Not. R. Astron. Soc. **355,** 424–443 (2004) doi:10.1111/j.1365-2966.2004.08334.x

Present-day scaling relations for submillimetre galaxies: the origin of spheroidal systems

T. Takagi,[1,2,3,4]★ H. Hanami[5] and N. Arimoto[6,7]

[1]*Centre for Astrophysics and Planetary Science, University of Kent, Canterbury, Kent CT2 7NR*
[2]*Blackett Laboratory, Imperial College, Prince Consort Road, London SW7 2BZ*
[3]*The Institute of Space and Astronautical Science, 3-1-1 Yoshinodai, Sagamihara, Kanagawa 229-8510, Japan*
[4]*Department of Physics, Rikkyo University, 3-34-1 Nishi-Ikebukuro, Toshima-ku, Tokyo 171-8501, Japan*
[5]*Physics Section, Faculty of Humanities and Social Sciences, Iwate University, Morioka, 020-8550, Japan*
[6]*Institute of Astronomy, School of Science, University of Tokyo, 2-21-1 Osawa, Mitaka, Tokyo 181-0015, Japan*
[7]*National Astronomical Observatory, 2-21-1 Osawa, Mitaka, Tokyo 181-8588, Japan*

Accepted 2004 August 18. Received 2004 August 16; in original form 2004 February 20

ABSTRACT

We analyse the spectral energy distributions (SEDs) of 23 submillimetre galaxies and three *ISO*-detected extremely red objects, all of which have the spectroscopic redshifts, using an evolutionary SED model of starbursts. This SED model allows us to investigate the intrinsic properties of starbursts, such as the starburst age and the mean stellar metallicity, as it consistently takes chemical evolution into account. Also, the intrinsic size of the starburst region is estimated from the observed SEDs. Using this SED model, we predict colours, magnitudes and sizes of present-day descendants of submillimetre galaxies to derive the scaling relations such as the colour–magnitude and size–magnitude relations. We argue that submillimetre galaxies are the progenitors of present-day elliptical galaxies, provided that the initial mass function (IMF) of submillimetre galaxies is slightly flatter than the Salpeter IMF. In this case, we find that: (1) the mean present-day magnitude of submillimetre galaxies is similar to that of L^* elliptical galaxies; (2) the present-day colour–magnitude relation is consistent with that of nearby elliptical galaxies; and (3) the present-day size–magnitude relation of elliptical galaxies can be reproduced if massive submillimetre galaxies consist of multiple starburst regions. Also, we find that starburst regions in submillimetre galaxies are likely to be self-regulated, i.e. the effect of feedback is nearly balanced by the self-gravity of starburst regions.

Key words: dust, extinction – galaxies: starburst – infrared: galaxies – submillimetre.

1 INTRODUCTION

Submillimetre galaxies are the key objects to understanding the process of galaxy formation (e.g. Smail, Ivison & Blain 1997; Hughes et al. 1998; Eales et al. 1999; Scott et al. 2002). It has been found that submillimetre galaxies are massive starburst galaxies at high redshifts, i.e. the gas mass is estimated to be as large as $\sim 10^{11}$ $M_\odot$ from the CO line emission measurements (Frayer et al. 1998, 1999; Ivison et al. 2001; Genzel et al. 2003; Neri et al. 2003), and the median redshift of $z = 2.4$ has recently been revealed spectroscopically (Chapman et al. 2003a). If the observed submillimetre fluxes originate mainly from star formation, the star formation rates (SFRs) of bright submillimetre galaxies are estimated to be over 10^3 $M_\odot$ yr^{-1} (e.g. Smail et al. 2002; Chapman et al. 2003a), large enough to produce a massive elliptical galaxy ($L > 3L^*$) within $\sim$1 Gyr (comparable to the Hubble time at $z = 2.5$). This estimate seems to be confirmed by follow-up observations at X-ray wavelengths, which suggest the negligible contribution of the active galactic nuclei (AGN) to submillimetre fluxes (Alexander et al. 2003). Also, submillimetre galaxies are sometimes found to be extended over $>$1 arcsec (e.g. Ivison et al. 2001). These observations indicate that submillimetre galaxies are the most plausible candidates as progenitors of present-day massive elliptical galaxies.

The evolutionary link between submillimetre galaxies and elliptical galaxies is also suggested by the statistical properties of submillimetre galaxies. The comoving number density of submillimetre galaxies with the 850-μm flux of $>$8 mJy is comparable to that of present-day ellipticals with $L \sim 3$–$4\ L^*$ (Chapman et al. 2003a). Another clue to the evolutionary link could be given by the clustering properties of submillimetre galaxies, which should be strong if they are the progenitors of massive elliptical galaxies. Actually, strong clustering of submillimetre galaxies is suggested by a large number of associations (Blain et al. 2004). This result may be confirmed by large submillimetre surveys in the near future.

Theoretically, the semi-analytic methods (SAMs) are extensively applied to explain the statistical properties of elliptical galaxies

★E-mail: t.takagi@kent.ac.uk

(e.g. Baugh, Cole & Frenk 1996; Kauffmann, Charlot & White 1996; Cole et al. 2000; Benson et al. 2001; Diaferio et al. 2001; Springel et al. 2001). The SAMs show that most of massive galaxies are formed at $z \lesssim 1$ as a result of successive mergings of smaller objects. Therefore, it is difficult to explain the statistical properties of submillimetre galaxies with the standard SAMs. This problem arises from the uncertainty in the relation between the dynamic evolution of the dark matter and the star formation processes in the early stage of galaxy formation (e.g. Binney 2004). In order to avoid this uncertainty, we may need an alternative method to investigate the evolutionary link between submillimetre galaxies and elliptical galaxies.

Elliptical galaxies are known as a fairly homogeneous family; for example, they exhibit very small scatter in the colour–magnitude (CM) relation (e.g. Bower, Lucy & Ellis 1992) and the relation between the Mg_2 index and the velocity dispersion σ (Dressler et al. 1987), i.e. their properties are well characterized as a sequence of mass. It is also remarkable that they occupy a two-dimensional sheet (fundamental plane) in the three-dimensional space defined by the velocity dispersion σ, the effective radius r_e and the mean surface brightness I_e within r_e (Djorgovski & Davis 1987; Dressler et al. 1987). If submillimetre galaxies evolve into elliptical galaxies, their present-day properties must be consistent with these scaling relations. This kind of test can provide another piece of evidence for the evolutionary link between submillimetre galaxies and elliptical galaxies.

In this paper, we analyse submillimetre galaxies using an evolutionary model of the spectral energy distribution (SED) for starburst galaxies, which is presented by Takagi, Arimoto & Hanami (2003a, hereafter TAH03). In this model, the chemical evolution of the starburst region is considered, i.e. if we specify the evolutionary phase of submillimetre galaxies as starbursts, the gas mass and the stellar mass of submillimetre galaxies can be estimated, together with their chemical properties. Also, the intrinsic size of the starburst region can be estimated from the observed SEDs, as the geometry of the starburst region determines its optical depth for a given dust mass. Using this model we predict the present-day colour, magnitude and size of submillimetre galaxies from observed SEDs, and produce the present-day scaling relations for submillimetre galaxies, i.e. the colour–magnitude and size–magnitude relations. Then, these scaling relations are compared with those of elliptical galaxies, in order to prove the evolutionary link between submillimetre galaxies and elliptical galaxies. This approach is new and complementary to previous studies.

The structure of this paper is as follows. We describe practical methods of SED diagnostics of submillimetre galaxies in Section 2. We summarize the results of SED fitting in Section 3. We confront the predicted present-day characteristics of submillimetre galaxies with those of present-day elliptical galaxies in Section 4. Then, we discuss a possible evolutionary scenario of submillimetre galaxies in Section 5. Our conclusions are given in Section 6. Throughout this paper, we adopt the cosmology of $\Omega_m = 0.3$, $\Omega_\Lambda = 0.7$ and $H_0 = 75$ km s^{-1} Mpc^{-1}.

2 PRESCRIPTION OF SED DIAGNOSTICS FOR SUBMILLIMETRE GALAXIES

2.1 Evolutionary SED model for submillimetre galaxies

We consider the evolution of starburst regions in submillimetre galaxies. Each starburst region is assumed to be a dynamically isolated system in which the chemical enrichment proceeds with effective mixing of gas by supernova feedback. The SED of such a starburst region is determined by the starburst age, for a given star formation history and the spatial distribution of stars and dust, i.e. its geometry. The adopted SED model is the same as that applied to nearby starbursts in TAH03, except for the initial metallicity and the initial mass function (IMF). Here we briefly describe this SED model.

2.1.1 *Evolutionary model of starburst regions*

We approximate the star formation history in a starburst region using the infall model of Arimoto, Yoshii & Takahara (1992). In this model, the overall star formation history is described with two time-scales, i.e. the gas infall time-scale t_i and the star formation time-scale t_*. We adopt the simplest case, in which a starburst is characterized by only one evolutionary time-scale t_0, i.e. we assume $t_i = t_* \equiv t_0$. Thus, we specify the star formation history by t_0, which is important only for the absolute time-scale of starburst events. Note that the chemical evolution as a function of t/t_0 is almost independent of the practical choice of t_0 (TAH03). As this is also true for the properties of the SED, specifically when $t_0 \gtrsim 50$ Myr, we can derive the chemical properties of starbursts from the observed SED, irrespective of the adopted value of t_0 (i.e. the star formation history). Practically, all models are calculated using $t_0 = 100$ Myr. Once the starburst age (t/t_0) is specified with a total mass of initial gas M_T from the SED fitting, we can derive the gas mass M_g and the stellar mass M_* in the starburst region, together with the metallicities of the gas and stars.

We assume that the initial metallicity of gas clouds Z_i is negligibly small (i.e. $Z_i = 0$). It is possible that gas clouds are initially enriched by the previous star formation activity. However, our conclusions are independent of the practical choice of Z_i as far as $Z_i \lesssim 0.1\,Z_\odot$.

A simple prescription of dust evolution is adopted, i.e. we assume that the dust-to-metal ratio δ_0 is constant. The value of δ_0 depends on the dust model. We adopt three dust models, i.e. the model for dust in the Milky Way (MW), the Large Magellanic Cloud (LMC) and the Small Magellanic Cloud (SMC). For the MW, LMC and SMC, the values of δ_0 derived from the extinction curve and the spectra of cirrus emission are 0.40, 0.55 and 0.75, respectively. See TAH03 and Takagi, Vansevičius & Arimoto (2003b) for more detailed descriptions.

2.1.2 *Geometry of starburst regions*

We assume that stars in submillimetre galaxies are centrally concentrated as for those in elliptical galaxies. The stellar density distribution is given by the King profile with $\log(R_t/R_c) = 2.2$, where R_t and R_c are the cut-off and core radius, respectively, and the adopted value is typical for elliptical galaxies (Combes et al. 1995). As in TAH03, dust is assumed to be distributed homogeneously within R_t.

TAH03 show that the effective radii of ultraluminous infrared galaxies (ULIRGs) derived from SEDs are consistent with the observed ones in the J, H and K bands. In this geometry, the longer the observed wavelengths, the smaller the observed effective radius, provided the observed flux is dominated by stellar emissions. This is because stars in the central region contribute to the observed flux more and more with decreasing optical depth. TAH03 also show that this trend is consistent with the observations of ULIRGs. Therefore, the adopted geometry is found to be suitable for nearby ULIRGs.

As the amount of dust is given by the chemical evolution, the geometry of the starburst region determines the optical depth due to

dust. Therefore, one of the important parameters of this SED model is the compactness factor Θ of starburst regions, defined by

$$\frac{R_{\rm t}}{1\ {\rm kpc}} = \Theta \left(\frac{M_*}{10^9\ {\rm M}_\odot} \right)^\gamma , \quad (1)$$

where $\gamma = \frac{1}{2}$ is adopted, resulting in a constant surface brightness for constant Θ. Note that the SED feature is preserved for different values of M_* when $\gamma = \frac{1}{2}$, as the source function within the starburst is conserved.

The optical depth of starburst regions, here defined with the column density of dust measured from the centre to the outer edge, is a function of the starburst age and Θ. Using M_* and Θ derived from the SED fitting, we calculate the intrinsic effective radius $R_{\rm e}$ (i.e. the effective radius with no dust),[1] which is given by 10.75 $R_{\rm c}$ in the adopted geometry.

In Section 4.2, we point out that massive submillimetre galaxies may consist of multiple starburst regions. Currently, photometric data are available only for a whole galaxy especially at longer wavelengths. Therefore, it is difficult to analyse the SED of each starburst region. If the SEDs of starburst regions in submillimetre galaxies are similar to each other, the derived starburst age and Θ for a whole galaxy can be interpreted as being those of each starburst region. This condition is such that each starburst is triggered almost simultaneously and the intrinsic bolometric surface brightness of each starburst region is similar to each other, such as nearby self-regulated starbursts (TAH03).

2.1.3 Evolution of stellar populations

A population synthesis code developed by Kodama & Arimoto (1997) is used to calculate the spectral evolution of stellar populations. In this model, the effects of stellar metallicity are explicitly taken into account in spectra. This is important to calculate consistently spectra of passively evolving galaxies, which mainly depend on the metallicity and the age of stellar population (Worthey 1994).

We adopt the two IMFs, i.e. the Salpeter IMF with the power-law index of $x = 1.35$ ($\rm IMF_{1.35}$), and a top-heavy IMF with the flatter slope $x = 1.10$ ($\rm IMF_{1.10}$). Such a flat IMF has been suggested by Kodama & Arimoto (1997) for elliptical galaxies, and found for the OB associations in the Milky Way (Massey, Johnson & Degioia-Eeastwood 1995). For both the IMFs, we adopt a lower and an upper mass limit of 0.1 and 60 $\rm M_\odot$, respectively.

The choice of IMF is important for the present-day magnitudes of submillimetre galaxies, as the mass-to-light ratio is smaller for the flatter IMF. Also, the present-day colours of submillimetre galaxies depend on the IMF, as the yield of chemical enrichment is higher for the flatter IMF (Arimoto & Yoshii 1986).

2.1.4 Radiative transfer with dust

The SED from ultraviolet (UV) to submillimetre wavelengths of the starburst region is calculated for each starburst age, Θ and the extinction curve (MW, LMC and SMC), using the radiative transfer code of TAH03. In this code, isotropic multiple scattering is assumed and the self-absorption of re-emitted energy from dust is fully taken into account. The temperature of dust grains is calculated for each dust size and constituent at each radial grid. For very small grains, the temperature fluctuation is calculated consistently with the radiative transfer (see Takagi et al. 2003b for details).

[1] Hereafter, we simply use the term 'effective radius' with this meaning in the remainder of the paper.

2.2 Sample galaxies

We consider submillimetre galaxies which have spectroscopic redshifts only, in order to minimize the uncertainty of the SED fitting.

The sample galaxies need to have extensive photometric data to be able to perform the SED fitting. We collect galaxies that have at least three photometric data values in the optical–near-infrared (NIR) bands.[2] In total, we find 23 galaxies detected at submillimetre wavelengths and three *ISO*-detected extremely red objects (EROs) from the literature (including private communications). For SMMJ02399-0136, we perform the SED fitting with two possible optical counterparts L1 and L2 (Ivison et al. 1998).

The sample includes EROs detected at the mid-infrared (MIR)–submillimetre wavelengths, submillimetre galaxies found in the SCUBA blank field surveys, submillimetre galaxies amplified by the gravitational lens, submillimetre galaxies in the protocluster region and host galaxies of GRBs detected at submillimetre wavelengths. Although three of the *ISO*-detected EROs do not have an observed flux at submillimetre wavelengths, we call the sample as submillimetre galaxies for simplicity.

The observed properties of the sample are given in Table 1 and we summarize the results of observations of the sample galaxies in Appendix A.

Note that we adopt the photometric data for whole galaxies. This may cause contamination from underlying stellar populations. It is expected that this contamination will be small for submillimetre galaxies, in which the gas mass is found to be comparable to that of massive galaxies (Frayer et al. 1998, 1999; Ivison et al. 2001; Genzel et al. 2003; Neri et al. 2003). Therefore, we assume that the contamination of underlying stellar populations, which is difficult to estimate from the currently available data, is negligible in submillimetre galaxies.

As the colour gradients are observed in submillimetre galaxies (e.g. Gear et al. 2000), the observed SEDs depend on the adopted aperture for photometry. Note that the SED model itself has colour gradients, because we solve the equations of radiative transfer. We use the model SEDs with the total aperture for consistency.

We assume that the SEDs of the submillimetre galaxies are dominated by starbursts, rather than AGN. It is found that most of submillimetre galaxies are X-ray faint, and therefore the contribution from AGN is not significant (Alexander et al. 2003). Consistently, some of the submillimetre galaxies are found to be extended in submillimetre and radio observations (e.g. Ivison et al. 2001). However, the contribution of AGN could be non-negligible at far-UV and MIR wavelengths, at which obscured starburst components have minimum luminosity. We discuss possible effects of the AGN contribution on the SED fitting analysis in Section 3.

2.3 SED fitting method

The best-fitting SED model is searched by the χ^2 minimization technique from a prepared set of SED models. We calculate the

[2] Although two gamma-ray burst (GRB) hosts have only two optical–NIR photometric data values, we find that the constraint on the model parameters is acceptable. This is because the observed SEDs are rather peculiar, which is reproduced only with very young and optically thick SED models. Therefore, we include these galaxies in the sample.

Table 1. Summary of observations of the sample.

Name	z	Amp.[a]	U (μJy)	B (μJy)	V (μJy)	R (μJy)	I (μJy)	J (μJy)	H (μJy)	K (μJy)	$S_{6.75\,\mu m}$ (mJy)	$S_{15\,\mu m}$ (mJy)	$S_{450\,\mu m}$ (mJy)	$S_{850\,\mu m}$ (mJy)	$S^{b}_{1.2-1.35\,mm}$ (mJy)	Ref.
HR10[c]	1.44	–	–	0.16	–	–	0.52[d]	6.4	14.8	27.7	–	0.203	32.3	4.89	2.13[e]	1, 2
EROJ164023	1.05	1.4	< 0.10	0.13	0.19	1.32[f]	3.00	20.4	21.3	63.0	–	0.530	–	< 6	–	3
ISOJ1324-2016	1.50	–	–	< 0.98	–	< 2.8	3.0	–	–	67.0	0.89	0.76	–	–	–	4
PDFJ011423[g]	0.65	–	–	–	3.02	11.1	–	91.4	–	485.0	4.1	7.6	–	–	–	5, 6
CUDSS14F	0.660	–	3.01	–	8.32	–	27.5	–	–	132.0	0.115	0.562	20.0	2.7	–	7, 8
CUDSS10A	0.550	–	–	–	1.74	–	12.0	–	–	100.0	–	–	23.0	4.8	–	7, 8
CUDSS14.13	1.15	–	0.97	1.2	2.5	–	16.4	–	–	155.0	0.613	1.653	–	3.3	–	9, 10, 11, 12
N2 850.1[a]	0.845	–	–	–	1.92	3.86	2.06	–	–	10.3	<1	< 2	23.0	11.2	–	13, 14
N2 850.2	2.45	–	–	–	< 0.16	0.39	0.21	–	–	7.9	<1	<2	35.0	10.7	–	13, 14, 15
N2 850.4	2.376	–	–	–	3.99	4.48	3.75	–	–	27.2	<1	< 2	< 34.0	8.2	2.59[h]	13, 14, 16
N2 850.8	1.189	–	–	–	2.78	5.79	3.09	–	–	35.2	<1	< 2	< 43.0	5.1	–	13, 14, 16
LE 850.6[i]	2.61	–	–	–	–	–	2.0	–	–	13.1	–	–	–	11.0	–	13, 15
SMMJ123600.2+621047	1.993	–	0.12	0.28	–	0.28	1.0	–	–	6.4	–	–	–	7.0	–	15, 17
SMMJ123629.13+621045.8	1.013	–	0.045	0.15	–	0.44	2.6	–	–	36.8	–	–	–	5.0	–	15
SMMJ123607.53+621550.4	2.415	–	0.41	1.6	–	1.1	2.0	–	–	12.2	–	–	–	4.0	–	15
SMMJ131212.7+424423	2.805	–	–	–	–	0.048	0.080	–	–	1.8	–	–	–	5.6	–	15, 17
SMMJ131201.2+424208	3.405	–	–	–	–	0.70	0.96	–	–	5.8	–	–	–	6.2	–	15, 17
SMMJ02399-0136[j] L1	2.80	2.5	0.153[k]	1.14	0.905	2.79	4.28	–	–	14.7	0.13	0.47	69.0	26.0	5.7[e]	18, 19
SMMJ02399-0136[j] L2	2.80	2.5	< 0.12[k]	0.320	0.205	0.518	0.653	–	–	1.19	0.13	0.47	69.0	26.0	5.7[e]	18, 19
SMMJ14011+0252 J1[l]	2.56	2.8	0.531	3.00	–	6.00	8.77	–	–	41.5	–	–	42.0	14.6	6.06[e]	20
SMMJ02399-0134[m]	1.06	2.5	4.45[n]	6.36	–	21.3	45.0	118.0	–	212.0	0.750	1.80	42.0	11.0	–	19, 21
SMMJ17142+5016	2.39	–	–	0.0875[d]	0.135[d]	–	0.205[d]	0.343[o]	0.956[o]	1.33	–	–	–	5.6	–	22, 23
SMMJ221726+0013	3.098	–	–	–	–	0.031	0.055	–	–	0.92	–	–	45.0	17.0	–	15, 24
SMMJ131225.7+424350	1.038	–	–	0.77	–	–	5.5	–	–	27.0	0.027	–	–	2.4	–	25
GRB000210	0.846	–	–	0.370	0.833	1.22	2.20	–	–	–	–	–	–	3.0	–	26, 27
GRB000418	1.119	–	–	–	–	1.1	–	–	–	1.7	–	–	41.0	3.2	–	27, 28
GRB010222	1.477	–	–	–	–	–	0.228[d]	–	–	0.445[p]	–	–	< 37.8	3.74	1.05[h]	29

Notes: [a]Amplification by gravitational lens. Flux densities in this table have not been corrected for gravitational amplifications. [b]Flux at millimetre wavelength, obtained with JCMT/SCUBA (1.35 mm) or IRAM/MAMBO (1.2 mm). [c]Additional photometry: $S_{12\,\mu m} = 0.85$ mJy and $S_{3.6cm} = 35$ μJy. [d]Photometry with *HST*/WFPC2: F300W for U, F450W for B, F606W for V, F814W for I. [e]Observed with JCMT/SCUBA at 1.35 mm. [f]Originally taken with the F702W band of *HST*/WFPC2. [g]Additional photometry: $S_{90\,\mu m} = 260$ mJy. [h]Observed with IRAM/MAMBO at 1.2 mm. [i]Additional photometry in the R band (S. Chapman, private communication). [j]Additional photometry: $S_{350\,\mu m}$<323 mJy, $S_{750\,\mu m} = 28$ mJy. [k]Originally taken with the F336W band of *HST*/WFPC2. [l]Additional photometry: $S_{3\,cm} < 1.8$ mJy. [m]Additional photometry: $S_{0.675\,\mu m} = 15.8$ μJy. [n]F336W band of *HST*/WFPC2. [o]Photometry with *HST*/NICMOS: F110W for J, F160W for H. [p]This flux is contaminated to some extent by the afterglow.

REFERENCES. (1) Dey et al. (1999), (2) Elbaz et al. (2002), (3) Smith et al. (2001) and references therein, (4) Pierre et al. (2001), (5) Afonso et al. (2001), (6) Georgakakis et al. (1999), (7) Lilly et al. (1999), (8) Eales et al. (1999), (9) Webb et al. (2003), (10) Clements et al. (2004), (11) Flores et al. (1999a), (12) Flores et al. (1999b), (13) Ivison et al. (2002), (14) Fox et al. (2002), (15) Chapman et al. (2004), private communication, (16) Chapman et al. (2003b), (17) Chapman et al. (2003a), (18) Ivison et al. (1998), (19) Smail et al. (2002), (20) Ivison et al. (2001), (21) Soucail et al. (1999), (22) Smail et al. (2003), (23) Keel et al. (2002), (24) Chapman et al. (2004), (25) Sato et al. (2004), (26) Piro et al. (2002), (27) Berger et al. (2003), (28) Berger et al. (2001) and (29) Frail et al. (2002).

SED models for 10 different starburst ages ($t/t_0 = 0.1$–6.0) and 16 different compactness factors ($\Theta = 0.3$–3.0) for each type of extinction curve, i.e. the best-fitting SED model is selected from a total of 480 SED models. This model set is made for both $\mathrm{IMF}_{1.35}$ and $\mathrm{IMF}_{1.10}$. The upper limits of flux are taken into account in the fitting process, i.e. models exceeding the 3σ upper limits are simply rejected.

3 RESULTS OF SED FITTING

The fitting results with $\mathrm{IMF}_{1.35}$ and $\mathrm{IMF}_{1.10}$ are summarized in Tables 2 and 3, respectively. The results of SED fitting are shown in Fig. 1 for $\mathrm{IMF}_{1.10}$ which is more suitable for submillimetre galaxies than $\mathrm{IMF}_{1.35}$ (see Section 4). Note that the fitting parameters are t/t_0 and Θ with the choice of the extinction curve. The normalization of the SED model is adjusted by M_{T}. The remaining quantities are derived from the best-fitting SED model. In Appendix B, we show the contour maps of $\Delta\chi^2$ for the sample used in the main analysis given in Sections 4 and 5. In addition, the typical values of estimated errors are shown in Figs 2, 4 and 6, below.

Table 4 summarizes the results of SED fitting, giving the number of galaxies for each bin of particular age and optical depth, and the resulting extinction curve. We find that 45 per cent of the submillimetre galaxies have $t/t_0 \leqslant 1$, in marked contrast to nearby starbursts, showing only ~ 23 per cent have $t/t_0 \leqslant 1$. Thus, a significant fraction of submillimetre galaxies are found to be young. The optical depth τ_V of submillimetre galaxies has a peak at 10–20, which is similar to that of nearby ULIRGs (cf. TAH03).

The large fraction of apparently young starbursts in submillimetre galaxies might be caused by an extra AGN contribution or the leakage of UV photons to the rest-frame UV light. As we have no further information on these effects in submillimetre galaxies, we hereafter assume that they are intrinsically young. This assumption does not change our main conclusions which are derived from old ($t/t_0 \geqslant 2.0$) submillimetre galaxies.

EROs detected in the MIR–submillimetre wavelengths are found to be the oldest starburst galaxies ($t/t_0 \gtrsim 5$) in the sample. This means that colours of stellar populations should be intrinsically red, in order to reproduce extremely red colours. Note that the derived stellar masses for EROs are systematically higher than those of the other sample, owing to the higher mass-to-light ratio.

GRB host galaxies (two out of three) have unique SEDs characterized by young stellar populations ($t/t_0 < 1$) and large optical depth ($\tau_V \sim 60$). Although their optical depths are the largest among our sample, the optical/NIR SEDs are not very red. This is because only stars near the surface of the starburst region actually contribute to the observed UV–NIR SED in such a large τ_V.

Spectroscopic observations and X-ray detections suggest that six sample galaxies (EROJ164023, ISOJ1324-2016, PDFJ011423, CUDSS14.13, SMMJ02399-0136 and SMMJ02399-0134) harbour AGNs. As a result of SED fitting, we find a clear MIR excess over the SED model for four sources (EROJ164023, PDFJ011423, CUDSS14.13 and SMMJ02399-0134), which can be attributed to hot dust components around AGNs. On the other hand, the observed MIR fluxes of the other sample (HR10, CUDSS14F and CUDSS14A) are reasonably explained solely by the starburst SED model. When the observed SEDs, except for the MIR excess, are well explained by the SED model, we assume that AGN dominates only at MIR wavelengths, and therefore the derived parameters are still usable for the subsequent analysis.

For four sample galaxies (EROJ164023, N2 850.1, SMMJ123629.13+621045.8, SMMJ131225.7+424350), we find no reasonable SED fit, i.e. SED models significantly underestimate the fluxes at MIR and submillimetre wavelengths even if they give a good fit to the optical–NIR SEDs. The possible reasons are: (1) the contamination from AGN (EROJ164023); (2) the uncertainty in the optical identification (N2 850.1); and (3) the low signal-to-noise ratio for faint objects (SMMJ131225.7+424350 with $S_{850\,\mu\mathrm{m}} = 2.4 \pm 0.74$ mJy). For SMMJ123629.13+621045.8, it seems that none of these reasons is suitable. Note that SMMJ123629.13+621045.8 is one of the reddest object ($R - K = 6.7$). We may need to extend the parameter range to fit such an extremely red SED. Accordingly, we exclude these four galaxies in the following analysis.

We present the fitting results of SMMJ02399-0136 for both L1 and L2. As the relative contribution to MIR–submillimetre flux from each component is uncertain due to the large beam size of the telescopes, we assumed that the observed MIR–submillimetre flux is dominated by either L1 or L2. If the observed dust emission is dominated by L2, the flux at a rest frame of 2 μm is significantly underestimated, while the flux at a rest frame of 4 μm is properly reproduced. It is difficult to explain this discrepancy by the presence of a hot dust component around the AGN. On the other hand, the SED of the L1 component is reproduced well by the model. Therefore, hereafter we assume that the observed dust emission originates mainly from the L1 component.

4 PRESENT-DAY SCALING RELATIONS OF SUBMILLIMETRE GALAXIES

4.1 Present-day colour–magnitude relation of submillimetre galaxies

The present-day colours and magnitudes are calculated under the assumption that the effects of star formation after the observed epoch are not significant for the resulting present-day colours and magnitudes. If a significant amount of cold gas is supplied into the system after the observed epoch, the effect of lasting star formation would contribute to the present-day colours and magnitudes. Therefore, this assumption is safe only for the starbursts in the later evolutionary phase; at $t/t_0 \sim 2$, approximately 60 per cent of the mass in the gas reservoir is already transformed into stars in the adopted gas infall model. A more detailed picture of star formation history of submillimetre galaxies is given in Section 5.1.

In Fig. 2, we compare the predicted present-day colours ($U - V$) and magnitudes of submillimetre galaxies with the colour–magnitude relation of nearby elliptical galaxies. In this figure, a solid curve with crosses indicates the present-day colour and magnitude of a starburst at $z = 3$ with $M_{\mathrm{T}} = 10^{12}\ \mathrm{M}_{\odot}$, which corresponds to the formation of the brightest elliptical galaxies. If the predicted present-day magnitude is lower than that indicated by this line at a given $U - V$, present-day descendants of submillimetre galaxies (or simply end-products) would be more massive than the brightest elliptical galaxies.

In the case of $\mathrm{IMF}_{1.35}$, more than half of old ($t/t_0 \geqslant 2$) submillimetre galaxies are more massive than the brightest elliptical galaxies. Moreover, the resulting $U - V$ colours of all sample galaxies are bluer than the CM relation. In order to redden the end-products, a significant number of metal-rich stars or old stars (i.e. red stars) should be supplied. As the stellar mass is already comparable to that of the brightest elliptical galaxies, such scenarios to supply red stars are not plausible. Therefore, we suggest that $\mathrm{IMF}_{1.35}$ is not appropriate for submillimetre galaxies.

On the other hand, in the case of $\mathrm{IMF}_{1.10}$, the majority of old submillimetre galaxies are less massive than the brightest

Table 2. The results of SED fitting with an IMF of $x = 1.35$.

Name	t/t_0	Θ	EC[b]	z	$\log M_{\rm T}^{c}$ ($M_\odot$)	τ_V	log SFR ($M_\odot$ yr^{-1})	$\log M_*$ ($M_\odot$)	$\log M_D$ ($M_\odot$)	$\log L_{\rm bol}$ ($L_\odot$)	$\log R_{\rm e}^{d}$ (pc)	M_V^{e}	M_B^{f}	$U-V^{g}$	$t_{z=0}^{h}$ (Gyr)	$\log\langle Z_*/Z_\odot\rangle_{z=0}^{i}$
HR10	5.0	0.3	SMC	1.44	11.94	15.3	2.74	11.91	9.20	12.74	2.76	−23.08	−22.11	1.30	9.0	−0.09
EROJ164023[a]	*6.0*	*0.5*	*MW*	*1.05*	*10.94*	*4.3*	*1.51*	*10.93*	*7.76*	*11.59*	*2.49*	*−20.72*	*−19.76*	*1.27*	*8.0*	*−0.06*
ISOJ1324-2016	5.0	0.3	SMC	1.50	12.42	15.3	3.22	12.39	9.68	13.22	3.00	−24.27	−23.30	1.30	9.2	−0.09
PDFJ011423	6.0	0.3	MW	0.65	12.21	11.9	2.78	12.20	9.03	12.86	2.91	−24.14	−23.20	1.22	6.2	−0.06
CUDSS14F	2.0	0.9	SMC	0.66	10.94	5.2	2.44	10.68	8.47	12.21	2.63	−20.52	−19.64	1.05	5.9	−0.38
CUDSS10A	5.0	0.3	MW	0.55	11.66	18.0	2.47	11.63	8.65	12.45	2.63	−22.84	−21.92	1.18	5.5	−0.10
CUDSS14.13	6.0	0.5	MW	1.15	12.02	4.3	2.58	12.00	8.84	12.67	3.03	−23.38	−22.41	1.28	8.3	−0.06
N2 850.1	*0.5*	*0.4*	*SMC*	*0.84*	*12.07*	*32.5*	*3.57*	*11.00*	*8.89*	*13.07*	*2.43*	*−21.66*	*−20.88*	*0.81*	*6.6*	*−1.05*
N2 850.2	5.0	0.3	SMC	2.45	12.32	15.3	3.12	12.29	9.58	13.12	2.95	−23.89	−22.90	1.34	10.6	−0.09
N2 850.4	0.5	0.7	LMC	2.38	12.44	8.9	3.93	11.36	9.11	13.44	2.86	−22.14	−21.34	0.84	10.1	−1.05
N2 850.8	0.7	0.7	SMC	1.19	11.87	10.8	3.42	11.03	8.92	13.03	2.69	−21.42	−20.60	0.90	7.9	−0.86
LE 850.6	0.3	0.7	SMC	2.61	12.90	8.9	4.25	11.44	9.25	13.66	2.89	−22.39	−21.66	0.72	10.3	−1.40
SMMJ123600.2+621047	6.0	0.3	MW	1.99	12.40	11.9	2.97	12.39	9.22	13.05	3.00	−24.17	−23.18	1.34	10.2	−0.06
SMMJ123629.13+621045.8[a]	*6.0*	*0.5*	*SMC*	*1.01*	*10.50*	*3.6*	*1.07*	*10.49*	*7.60*	*11.16*	*2.27*	*−19.64*	*−18.68*	*1.27*	*7.8*	*−0.06*
SMMJ123607.53+621550.4	1.0	1.2	MW	2.42	11.80	4.3	3.39	11.19	8.80	13.04	3.00	−21.48	−20.60	1.01	10.2	−0.68
SMMJ131212.7+424423	5.0	0.3	SMC	2.81	11.89	15.3	2.69	11.86	9.15	12.69	2.74	−22.79	−21.80	1.35	11.0	−0.09
SMMJ131201.2+424208	0.5	0.9	LMC	3.40	12.35	5.4	3.84	11.27	9.02	13.35	2.92	−21.85	−21.05	0.85	10.9	−1.05
SMMJ02399-0136 L1	0.5	0.7	LMC	2.80	12.45	8.9	3.94	11.38	9.12	13.45	2.86	−22.14	−21.34	0.85	10.5	−1.05
SMMJ02399-0136 L2[a]	*0.3*	*0.3*	*LMC*	*2.80*	*12.69*	*40.8*	*4.04*	*11.23*	*8.91*	*13.42*	*2.42*	*−21.86*	*−21.12*	*0.72*	*10.5*	*−1.40*
SMMJ14011+0252 J1	1.0	1.4	MW	2.56	11.85	3.2	3.44	11.24	8.86	13.09	3.10	−21.60	−20.73	1.01	10.3	−0.68
SMMJ02399-0134	1.0	1.0	SMC	1.06	11.55	5.3	3.15	10.95	8.83	12.82	2.80	−21.15	−20.30	0.97	7.5	−0.69
SMMJ17142+5016	3.0	0.4	LMC	2.39	11.72	15.7	3.01	11.60	9.10	12.85	2.73	−22.24	−21.28	1.27	10.4	−0.23
SMMJ221726+0013	2.0	0.3	SMC	3.10	11.84	46.7	3.33	11.58	9.37	13.09	2.60	−22.22	−21.28	1.19	10.9	−0.37
SMMJ131225.7+424350[a]	*3.0*	*1.0*	*LMC*	*1.04*	*10.62*	*2.5*	*1.91*	*10.50*	*7.99*	*11.75*	*2.58*	*−19.74*	*−18.81*	*1.18*	*7.7*	*−0.23*
GRB000210	4.0	0.3	SMC	0.85	11.55	22.9	2.60	11.49	8.96	12.51	2.55	−22.27	−21.33	1.20	7.0	−0.15
GRB000418	0.3	0.3	MW	1.12	12.51	57.3	3.86	11.05	8.59	13.22	2.33	−21.71	−20.98	0.71	7.7	−1.39
GRB010222	0.3	0.3	MW	1.48	12.44	57.3	3.79	10.98	8.52	13.15	2.30	−21.39	−20.66	0.70	8.6	−1.40

Notes: [a]Submillimetre galaxies unused in Sections 4 and 5. [b]Extinction curve. [c]Initial mass of gas reservoir. [d]Intrinsic effective radius. [e]Present-day V-band absolute magnitude of submillimetre galaxies. [f]Present-day B-band absolute magnitude of submillimetre galaxies. [g]Present-day $U-V$ for submillimetre galaxies. [h]Age of submillimetre galaxies at $z=0$ when $t_0 = 100$ Myr. [i]Mean luminosity-weighted metallicity of stars.

Table 3. The results of SED fitting with an IMF of $x = 1.10$.

Name	t/t_0	Θ	EC[b]	z[c]	$\log M_{\rm T}^{d}$ ($M_\odot$)	τ_V	log SFR ($M_\odot$ yr^{-1})	$\log M_*$ ($M_\odot$)	$\log M_D$ ($M_\odot$)	$\log L_{\rm bol}$ ($L_\odot$)	$\log R_{\rm e}^{e}$ (pc)	M_V^{f}	M_B^{g}	$U-V$[h]	$t^{i}_{z=0}$ (Gyr)	$\log\langle Z_*/Z_\odot\rangle^{j}_{z=0}$
HR10	6.0	0.5	SMC	1.44	11.67	14.8	2.47	11.64	9.34	12.63	2.85	−22.26	−21.18	1.64	9.1	0.35
EROJ164023[a]	*6.0*	*0.9*	*SMC*	*1.05*	*10.36*	*4.5*	*1.16*	*10.34*	*8.04*	*11.32*	*2.45*	*−19.13*	*−18.06*	*1.60*	*8.0*	*0.36*
ISOJ1324-2016	4.0	0.7	SMC	1.50	12.04	14.5	3.23	11.96	9.95	13.30	3.16	−23.06	−21.99	1.58	9.1	0.25
PDFJ011423	6.0	0.7	MW	0.65	11.81	8.9	2.60	11.78	9.20	12.75	3.07	−23.00	−21.95	1.53	6.2	0.35
CUDSS14F	2.0	1.6	SMC	0.66	10.70	4.8	2.25	10.40	8.65	12.25	2.74	−19.68	−18.72	1.29	5.9	0.00
CUDSS10A	6.0	0.5	MW	0.55	11.56	17.4	2.35	11.53	8.95	12.50	2.79	−22.47	−21.43	1.50	5.6	0.34
CUDSS14.13	6.0	0.9	LMC	1.15	11.60	3.8	2.39	11.57	9.13	12.55	3.07	−22.16	−21.09	1.61	8.3	0.36
N2 850.1[a]	*2.0*	*2.4*	*SMC*	*0.84*	*9.60*	*2.1*	*1.16*	*9.31*	*7.55*	*11.16*	*2.37*	*−16.80*	*−15.83*	*1.32*	*6.8*	*0.01*
N2 850.2	5.0	0.7	SMC	2.45	11.86	10.5	2.85	11.81	9.66	12.96	3.08	−22.53	−21.44	1.66	10.6	0.30
N2 850.4	0.7	2.2	MW	2.38	11.90	3.4	3.47	11.03	9.06	13.35	3.19	−20.97	−20.07	1.10	10.1	−0.50
N2 850.8	0.5	1.0	SMC	1.19	11.87	12.9	3.37	10.76	9.04	13.22	2.71	−20.66	−19.81	0.96	7.9	−0.70
LE 850.6	1.0	1.4	LMC	2.61	11.87	6.1	3.49	11.23	9.40	13.42	3.09	−21.35	−20.40	1.22	10.4	−0.31
SMMJ123600.2+621047	6.0	0.7	MW	1.99	11.83	8.9	2.63	11.80	9.23	12.78	3.08	−22.56	−21.47	1.67	10.2	0.34
SMMJ123629.13+621045.8[a]	*6.0*	*1.0*	*SMC*	*1.01*	*10.16*	*3.7*	*0.96*	*10.14*	*7.84*	*11.12*	*2.40*	*−18.65*	*−17.58*	*1.59*	*7.8*	*0.37*
SMMJ123607.53+621550.4	1.0	2.0	MW	2.42	11.49	4.2	3.11	10.84	8.88	13.02	3.05	−20.41	−19.47	1.22	10.2	−0.31
SMMJ131212.7+424423	6.0	0.5	SMC	2.81	11.66	14.8	2.45	11.63	9.33	12.61	2.84	−22.03	−20.93	1.69	11.1	0.34
SMMJ131201.2+424208	0.5	1.4	LMC	3.40	11.99	5.5	3.49	10.88	9.02	13.34	2.92	−20.65	−19.78	1.00	10.9	−0.70
SMMJ02399-0136 L1	0.3	0.9	LMC	2.80	12.45	11.3	3.81	10.96	9.04	13.52	2.77	−21.06	−20.27	0.84	10.5	−1.03
SMMJ02399-0136 L2[a]	*0.3*	*0.4*	*LMC*	*2.80*	*12.43*	*57.2*	*3.79*	*10.94*	*9.01*	*13.47*	*2.40*	*−21.01*	*−20.22*	*0.84*	*10.5*	*−1.03*
SMMJ14011+0252 J1	1.0	2.4	MW	2.56	11.52	2.9	3.13	10.87	8.91	13.05	3.15	−20.47	−19.52	1.22	10.3	−0.31
SMMJ02399-0134	2.0	1.6	LMC	1.06	11.11	4.0	2.67	10.82	8.92	12.66	2.94	−20.45	−19.47	1.35	7.6	0.01
SMMJ17142+5016	3.0	0.7	LMC	2.39	11.46	16.4	2.85	11.31	9.30	12.87	2.83	−21.33	−20.28	1.56	10.4	0.15
SMMJ221726+0013	6.0	0.3	SMC	3.10	12.08	41.0	2.87	12.05	9.75	13.02	2.83	−23.05	−21.96	1.69	11.3	0.34
SMMJ131225.7+424350[a]	*2.0*	*2.0*	*SMC*	*1.04*	*10.26*	*3.1*	*1.82*	*9.97*	*8.21*	*11.81*	*2.62*	*−18.33*	*−17.35*	*1.34*	*7.6*	*0.01*
GRB000210	5.0	0.7	MW	0.85	11.39	12.4	2.38	11.35	8.92	12.48	2.85	−21.77	−20.72	1.55	7.1	0.33
GRB000418	0.3	0.5	MW	1.12	12.13	51.5	3.49	10.65	8.58	13.16	2.35	−20.59	−19.81	0.81	7.7	−1.03
GRB010222	0.5	0.4	LMC	1.48	11.65	67.8	3.15	10.54	8.68	12.96	2.21	−20.02	−19.17	0.97	8.7	−0.70

See notes in Table 2.

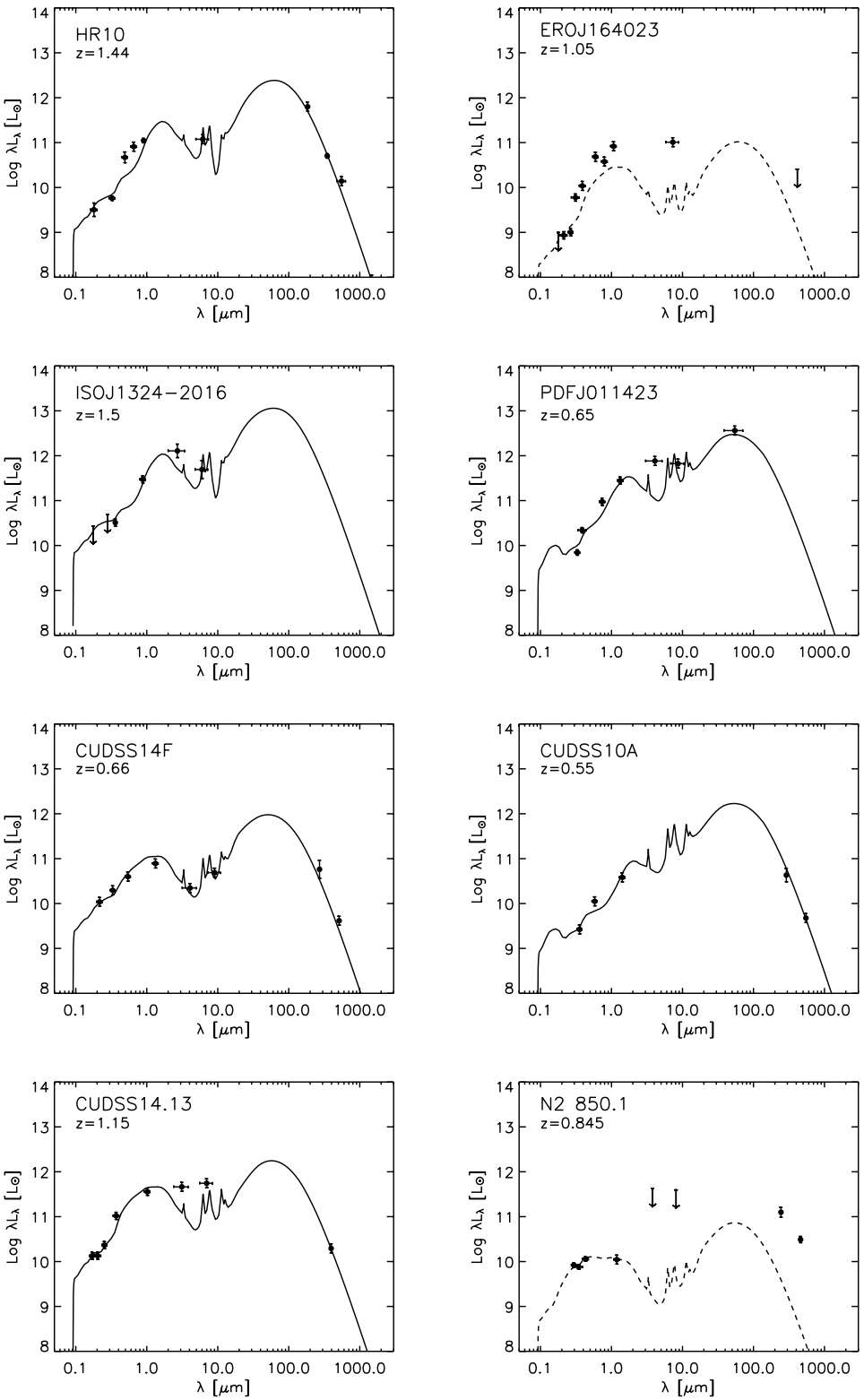

Figure 1. Results of SED fitting with the IMF of $x = 1.10$ in the rest frame. The references for data are given in Table 1. Galaxies for which the SED model is indicated by a dashed line are unused in the subsequent analysis (Sections 4 and 5).

elliptical galaxies. We derive the mean $V(B)$-band magnitude of -22.03 (-20.97) mag for old submillimetre galaxies. Thus, the typical luminosity of the end-products of these submillimetre galaxies is similar to those of L^* elliptical galaxies which have $M_B^* = -20.75$ mag (Marinoni et al. 1999).

For $\mathrm{IMF}_{1.10}$, not only the magnitudes, but also the present-day colours of old submillimetre galaxies become consistent with those of elliptical galaxies, i.e. old submillimetre galaxies seem to follow the CM relation. This suggests that these submillimetre galaxies can be real progenitors of elliptical galaxies.

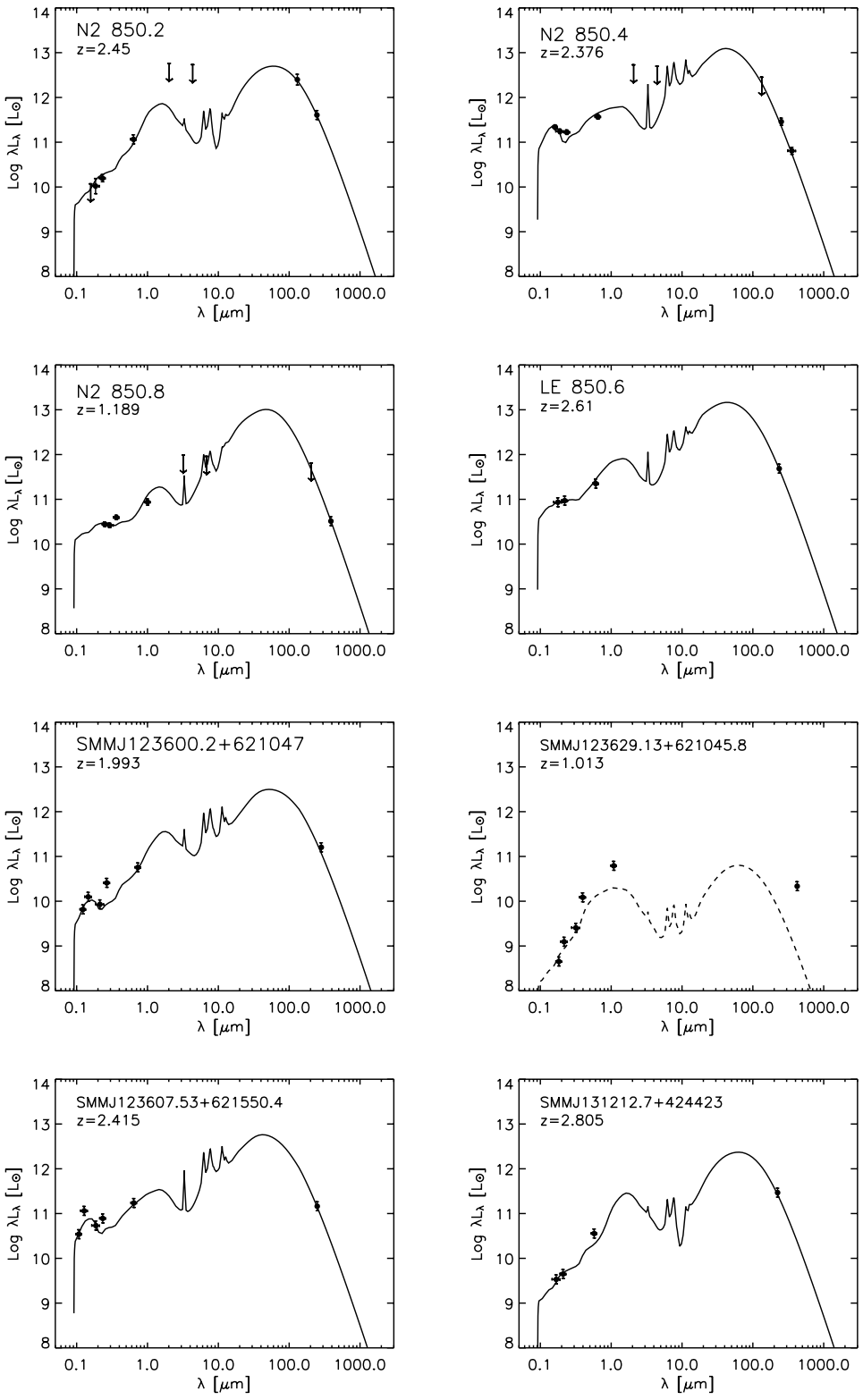

Figure 1 – *continued*

Note that young ($t/t_0 < 2$) submillimetre galaxies are systematically bluer than old ($t/t_0 \geqslant 2$) ones. This is because we assume that the star formation ceases at the observed epoch, irrespective of derived starburst ages, and therefore the mean metallicity of stars in young submillimetre galaxies is smaller than that of old ones.

The observations of passively evolving elliptical galaxies suggest that the origin of the CM relation is the systematic difference in the mean metallicity of stars (Kodama & Arimoto 1997). Here we can check the origin of the CM relation independently of the previous studies. In Fig. 3, we show the present-day age and the

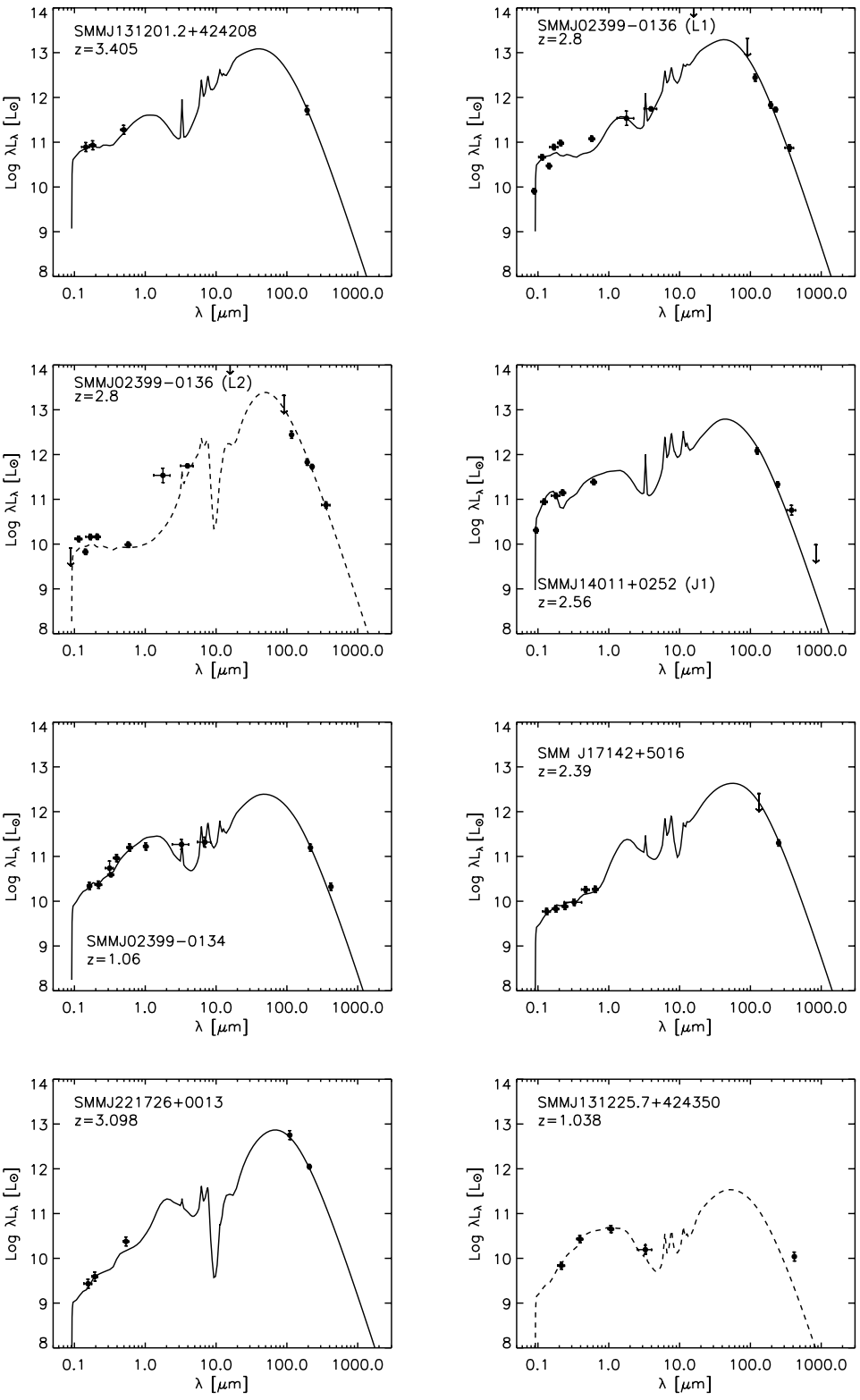

Figure 1 – *continued*

luminosity-weighted metallicity as a function of the present-day V-band magnitude. The scatter of age is considerable at all magnitudes. Such a large dispersion in age has recently been confirmed by Yamada, Arimoto & Vazdekis (in preparation) for elliptical galaxies in the field with a detailed study of the Hγ_σ absorption index (Vazdekis & Arimoto 1999). Therefore, three luminous submillimetre galaxies ($M_V \leqslant -21.5$) with ages of < 8 Gyr and $z \leqslant 0.85$ could be real progenitors of young field ellipticals. In Table 5, we give the mean characteristics of old submillimetre galaxies at $z = 0$ for each bright ($M_V < -22$) and a faint sample ($M_V \geqslant -22$). Although

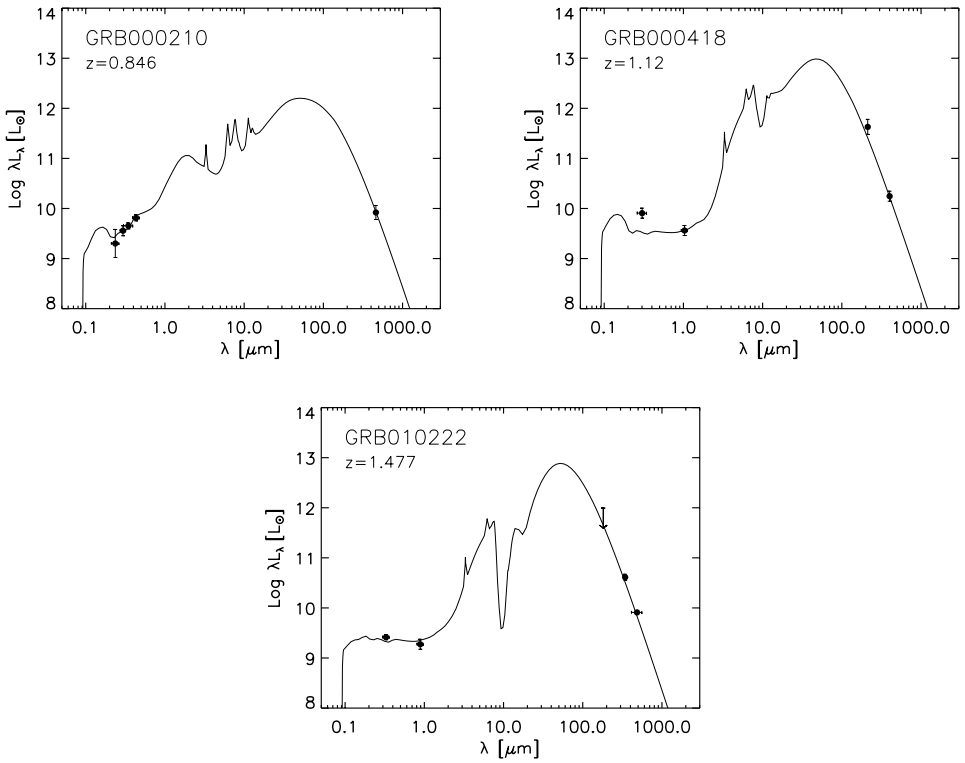

Figure 1 – *continued*

Table 4. Number of submillimetre galaxies at each fitting parameter bin.

Age	$IMF_{1.35}$	IMF1.10
$t/t_0 \leqslant 1$	10	10
$t/t_0 = 2$	2	2
$t/t_0 = 3$	1	1
$t/t_0 = 4$	1	1
$t/t_0 = 5$	5	2
$t/t_0 = 6$	3	6
Optical depth		
$\tau_V \leqslant 3.0$	0	1
$3 < \tau_V \leqslant 5.0$	3	3
$5 < \tau_V \leqslant 10.0$	6	4
$10 < \tau_V \leqslant 20.0$	9	9
$\tau_V > 20.0$	4	3
Extinction curve		
MW	8	8
LMC	4	7
SMC	10	7

Note: we exclude EROJ164023, N2 850.1, SMMJ123629.13+621045.8 and SMMJ131225.7+424350, for which we find no reasonable SED fit.

faint sample of old submillimetre galaxies appears to give a young mean value, we find no difference in the mean age when we include young submillimetre galaxies (open circles in Fig. 3). Note that the present-day age depends mainly on the redshift, not on the starburst age, while the present-day magnitude depends on the starburst age. If the end-products of young submillimetre galaxies remain faint ($M_V \geqslant -22$), there is no systematic difference in the present-day age between the bright and the faint sample. On the other hand, we find a systematic difference in the mean luminosity-weighted metallicity, $\Delta\log\langle Z_*/Z_\odot\rangle = 0.19$. Thus, the CM relation of elliptical galaxies could be caused by a systematic difference in the metallicity. However, we need a fainter sample of old submillimetre galaxies to derive firm conclusions regarding this issue.

The analyses of the observed CM relation of elliptical galaxies suggest that major star formation for elliptical galaxies occurred at $z > 2$ (e.g. Bower, Lucy & Ellis 1992; Kodama et al. 1998; Stanford, Eisenhardt & Dickinson 1998). This suggests that the progenitor of elliptical galaxies would be found mostly at $z \gtrsim 2$. On the other hand, the mean redshift of our sample is 1.6, while recent spectroscopic observations of submillimetre galaxies suggest a median redshift of $z \sim 2.4$ (Chapman et al. 2003a). Our sample is likely to be biased towards low redshifts, as they should be bright enough in the optical/NIR photometric bands to perform spectroscopic observations and SED fitting. Therefore, our sample occupies the lower tail of the redshift distribution of submillimetre galaxies. Nevertheless, the present-day colours and magnitudes of the sample are consistent with the observed CM relation. This suggests that the physical mechanisms to establish the CM relation are still effective even at $z \lesssim 2$.

4.2 The present-day size–magnitude relation of submillimetre galaxies

We compare the present-day *B*-band magnitudes and effective radii of submillimetre galaxies with the observed relation for elliptical galaxies, the so-called the Kormendy relation. As $IMF_{1.10}$ is more suitable for submillimetre galaxies as shown above, we mainly focus on this case. The effective radii of old submillimetre galaxies range from ~ 300 pc to a few kpc. As shown in Fig. 4(a), the predicted effective radii of less massive galaxies with $M_B \sim -19$ mag are consistent with the observed ones, while those of massive galaxies are an order of magnitude smaller than the observed ones.

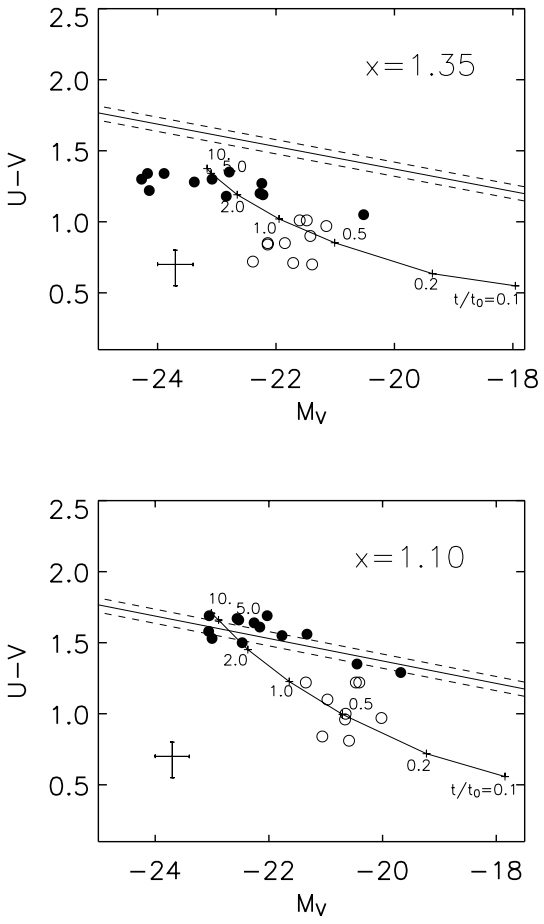

Figure 2. The predicted colours and magnitudes of submillimetre galaxies at the present epoch. Open and solid circles indicate the sample galaxies with an age of $t/t_0 \leqslant 1.0$ and those of $t/t_0 > 1.0$, respectively. The solid straight line is for the regression line to the CM relation observed in the Coma cluster derived by Bower et al. (1992), and dashed lines indicate the observed scatter ± 0.05 mag. The depicted loci with starburst age indicate the colours and magnitudes of starburst galaxies formed at $z \sim 3$ with the mass of gas reservoir $M_{\rm T} = 10^{12}\,{\rm M}_{\odot}$, in which the star formation ceases at the indicated starburst age. Note that a starburst galaxy with $M_{\rm T} = 10^{12}\,{\rm M}_{\odot}$ becomes a passively evolving galaxy with $M_V = -23$, i.e. a typical brightest elliptical galaxy when $x = 1.10$ and the star formation ceases at a starburst age of $t/t_0 = 5.0$ We show the typical errors at the lower left-hand corner.

This discrepancy in $R_{\rm e}$ for massive galaxies can be explained if the starburst region in submillimetre galaxies is a multiple system rather than a unit system, i.e. several starburst regions are distributed within the potential of a whole galaxy, and these starburst regions eventually merge to form a more diffuse stellar system. Note that recent observations of submillimetre galaxies with the *Hubble Space Telescope* (*HST*) actually show multiple structures (Chapman et al. 2003b). As we note in Section 2.1.2, the interpretation of the SED fitting remains the same if each starburst region is triggered almost simultaneously, and the intrinsic bolometric surface brightness of each starburst region is similar to each other.

The other possibility which may account for this discrepancy is that the stellar system expands, owing to the dynamic response to gas removal as a galactic wind. Following Yoshii & Arimoto (1987), we find that old submillimetre galaxies could expand by no more than a factor of ~ 3, irrespective of the time-scale of gas removal. Moreover, this effect is expected to be more significant for less massive galaxies. However, the discrepancy of the effective radius between submillimetre galaxies and elliptical galaxies is larger for more massive submillimetre galaxies. Therefore, it is difficult to explain the discrepancy of $R_{\rm e}$ only by the dynamic response of a stellar system to gas removal.

The size–magnitude relation of submillimetre galaxies seems to deviate from that of elliptical galaxies around $M_B \sim -19.5$ mag, i.e. the largest starburst regions in submillimetre galaxies probably have the present-day magnitude of only $M_B \sim -19.5$ mag. The number of starburst regions can be estimated from the present-day magnitudes if submillimetre galaxies with the present-day $M_B = -19.5$ mag are the largest starburst regions. This means that submillimetre galaxies with the L^* present-day luminosity are likely to have at least approximately three starburst regions within a size of effective radius ~ 5 kpc. The clumpiness of submillimetre galaxies may correlate with the mass of submillimetre galaxies, as the discrepancy of the radius is larger for more massive submillimetre galaxies. It is important to confirm the existence of the maximum scale in starburst regions, in order to understand the star formation process at high redshifts. To do this, we need high-resolution imaging, e.g. with the Atacama Large Millimeter Array (ALMA).

If submillimetre galaxies consist of multiple starburst regions, we need to correct the derived $R_{\rm e}$ for the multiplicity and for the effect of merging of these starburst regions, in order to compare the derived $R_{\rm e}$ with the effective radius of elliptical galaxies. To

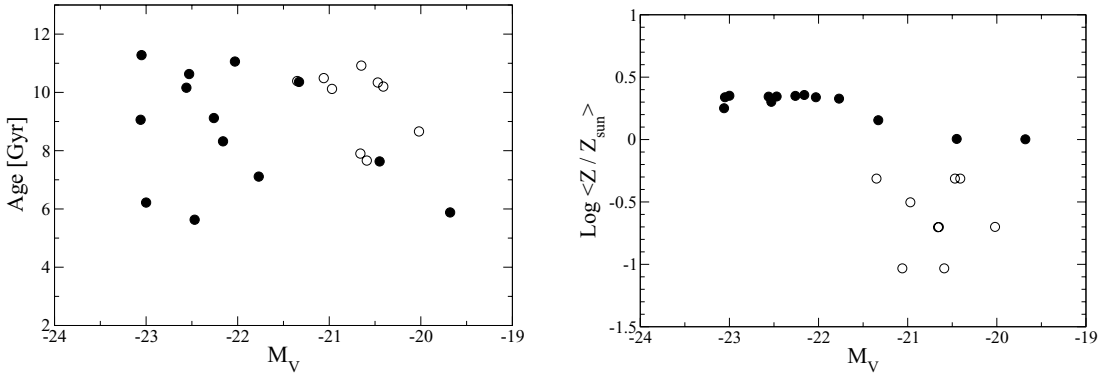

Figure 3. The present-day age and luminosity-weighted stellar metallicity of submillimetre galaxies. The symbols are the same as those used in Fig. 2. The IMF of $x = 1.10$ is adopted. Left-hand panel: the present-day ages are plotted as a function of the present-day M_V. The present-day ages are calculated from the look-back time plus the starburst age assuming $t_0 = 100$ Myr; right-hand panel: the luminosity-weighted stellar metallicities are plotted as a function of present-day M_V.

Table 5. The mean characteristics of old submillimetre galaxies at $z = 0$.

	Sample	$\langle z \rangle$	$\langle M_V \rangle$	$\langle U - V \rangle$	$\langle t_{z=0} \rangle$ (Gyr)	$\langle \log \langle Z_*/Z_\odot \rangle \rangle$
Bright samples ($M_V < -22$)	9	1.7	−22.57	1.62	9.0 (9.0)[a]	0.33
Faint samples ($M_V > -22$)	4	1.2	−20.81	1.44	7.7 (9.0)[a]	0.14
All samples	13	1.6	−22.03	1.56	8.64	0.27

Note: the mean values are given for old submillimetre galaxies ($t/t_0 \geqslant 2$). All the values are derived with the IMF of $x = 1.10$. (a) The mean of the present-day age including young submillimetre galaxies.

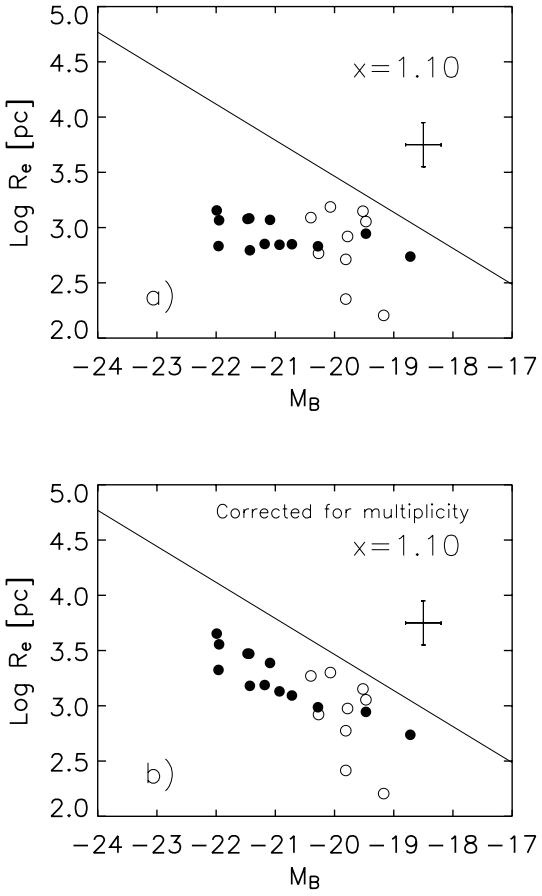

Figure 4. (a) Comparison of B-band magnitudes and effective radii with the observed size–magnitude relation of elliptical galaxies (solid line) obtained from the sample of Bender, Burstein & Faber (1992). The symbols are the same as those in Fig. 2. The typical errors are shown. (b) Same as (a), but corrected for multiplicity (see the text for details).

estimate the correction factor for these effects, we simply assume that starburst regions in a submillimetre galaxy have a similar mass and SED to each other. We call this assumption the 'equality' condition of the starburst region. Hereafter, we denote the stellar mass and the effective radius of each starburst region as m_* and r_e, respectively. When a submillimetre galaxy consists of N starburst regions, we can write $r_e \sim R_e/\sqrt{N}$, as $m_* = M_*/N$ and $R_e \propto (Nm_*)^{1/2}$. The gravitational energy per unit mass in a starburst region is $Gm_*/r_e \sim GM_*/\sqrt{N}R_e$. If the gravitational energy per unit mass does not change during the assembly process of multiple starburst regions, and the total stellar mass is conserved, massive submillimetre galaxies would eventually evolve into elliptical galaxies with an effective radius of $\sim \sqrt{N}R_e$, i.e. we need the correction factor of $\sqrt{N}$ for the effective radii in Fig. 4(a). In Fig. 4(b), we show the size–magnitude relation corrected for the multiplicity. Note that the corrected size–magnitude relation has a similar slope to the observed size–magnitude relation of elliptical galaxies. The zero point is marginally consistent with the observation within the uncertainty, although it is systematically lower by a factor of ~ 2. The difference in the zero point might be explained by the expansion of the stellar system, as a result of gas removal from each starburst region at the end of its activity (e.g. Yoshii & Arimoto 1987).

5 EVOLUTION OF SUBMILLIMETRE GALAXIES

The starburst activity can be characterized by the relative strength of self-gravity to feedback (TAH03). In massive and compact starbursts such as nearby ULIRGs, the self-gravity of the starburst region becomes strong enough to suppress the feedback effect. This is because the supernova rate depends mainly on the total baryonic mass of starburst regions, while the self-gravity increases with decreasing size of starburst region for a given mass. First, we investigate the relative strength of self-gravity to feedback in submillimetre galaxies, which can provide an insight into the evolution of submillimetre galaxies.

5.1 Feedback versus self-gravity in submillimetre galaxies

The total kinetic energy of gas due to feedback with the typical velocity V_g can be written as $\frac{1}{2}M_g V_g^2 \simeq L_{kin}t_{dyn}$, where L_{kin} is the kinetic luminosity due to feedback and t_{dyn} is the dynamic timescale of the system. Assuming that $L_{kin} = f_{kin}L_{bol}$ and $t_{dyn} = t_0$, the kinetic energy per a unit mass can be written as

$$\frac{1}{2}V_g^2 \simeq \frac{L_{kin}t_{dyn}}{M_g} = f_{kin}\frac{L_{bol}}{\psi}, \tag{2}$$

where ψ ($= M_g/t_0$) is the SFR. We use the relation

$$\frac{L_{bol}}{\varepsilon L_\odot} = \frac{\psi}{1\,M_\odot\,yr^{-1}}\left(\frac{t}{t_0}\right)^\alpha, \tag{3}$$

where we find $\varepsilon = (1.7 \times 10^9, 7.0 \times 10^9)$ and $\alpha = (1.0, 0.42)$ for $IMF_{1.35}$ and $IMF_{1.10}$. Then, we derive the escape velocity, $V_{esc}^2 \simeq 2GM(<R_e)/R_e$, where $M(<R_e)$ is the total mass within R_e. Here, we simply assume $f_{kin} = 0.01$ and $M(<R_e) = 2M_*(<R_e)$ as in TAH03. The limiting effect of feedback against self-gravity can be estimated by the comparison of V_g with V_{esc}. These velocities should be corrected when submillimetre galaxies consist of N starburst regions. For the equality condition of starbursts, we find the escape velocity of each starburst region $v_{esc}^2 \simeq V_{esc}^2/\sqrt{N}$, as $m_* = M_*/N$ and $r_e \simeq R_e/\sqrt{N}$. On the other hand, we expect the velocity of gas due to feedback in each starburst to be $v_g \simeq V_g$, as the strength of the feedback mainly depends on the efficiency of star formation, not on the mass scale. Therefore, we find $v_g^2/v_{esc}^2 \simeq \sqrt{N}V_g^2/V_{esc}^2$. If starbursts are self-regulated, we expect $v_g^2/v_{esc}^2 \gtrsim 1$.

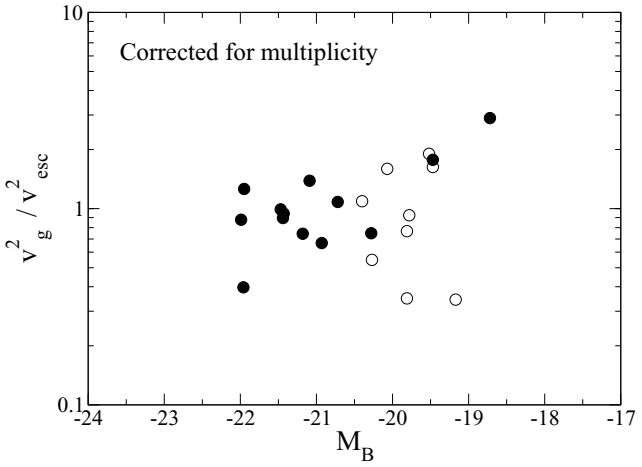

Figure 5. The comparison of the gas velocity by feedback with the escape velocity as a function of the present-day B magnitude with the IMF of $x = 1.10$. The symbols are the same as those in Fig. 2. The squared velocity ratio is corrected for the multiplicity. See the text for details.

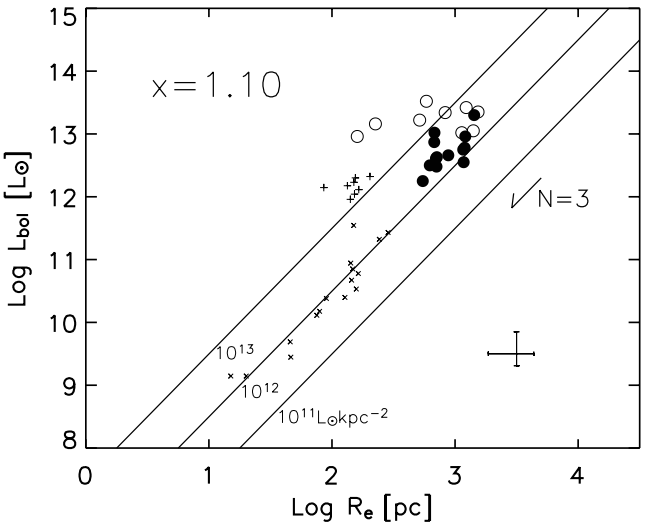

Figure 6. The bolometric luminosities of the sample galaxies plotted against the intrinsic effective radii derived from the SED fitting. Crosses (×) and plus signs (+) indicate UVSBGs and ULIRGs, taken from TAH03. The other symbols are the same as those used in Fig. 2. We indicate the correction factor for the multiplicity with an arrow for the case of $N = 3$. The typical errors are shown.

In Fig. 5, we show v_g^2/v_{esc}^2 corrected for the multiplicity, and find that most of the old submillimetre galaxies have $v_g^2/v_{esc}^2 \sim 1$. This suggests that feedback is effective, and therefore the star formation in old submillimetre galaxies is likely to be self-regulated.

In the local Universe, TAH03 suggest that UV-selected starburst galaxies (UVSBGs) are self-regulated, while ULIRGs are dynamically unstable. The difference between UVSBGs and ULIRGs can be seen as a systematic difference in the intrinsic bolometric surface brightness. In Fig. 6, we show the bolometric luminosity L_{bol} and the effective radius R_e of submillimetre galaxies, along with those of nearby starburst galaxies. An arrow in Fig. 6 indicates the correction due to the multiplicity, assuming the equality condition of starbursts and $N = 3$. The intrinsic bolometric surface brightness of old submillimetre galaxies are systematically lower than those of

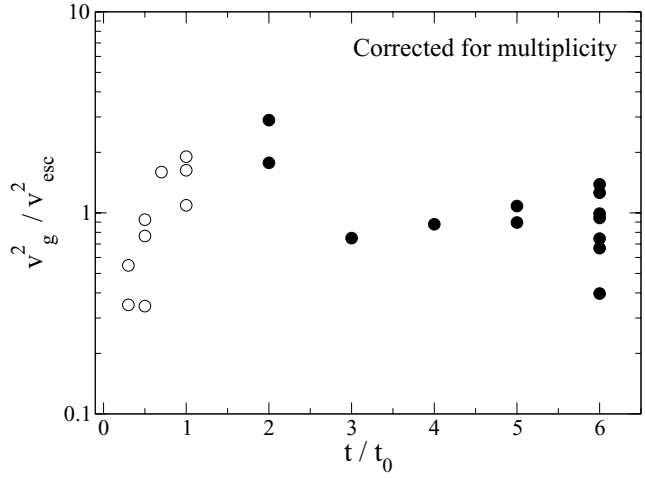

Figure 7. The squared velocity ratio as a function of the starburst age with the IMF of $x = 1.10$. The symbols are the same as those in Fig. 2. The squared velocity ratio is corrected for the multiplicity. See the text for details.

nearby ULIRGs that have $>10^{13}$ $L_\odot$ kpc^{-2}; instead, it seems to follow the relation of UVSBGs. Again, this may indicate that old submillimetre galaxies are self-regulated starbursts. Thus, the effect of feedback could be very important for the evolution of submillimetre galaxies.

5.2 Role of feedback and origin of the CM relation

The evolutionary trend of the feedback effect in submillimetre galaxies can be seen in Fig. 7, which shows v_g^2/v_{esc}^2 for submillimetre galaxies (corrected for the multiplicity) as a function of starburst age t/t_0. For old submillimetre galaxies, v_g^2/v_{esc}^2 is found to be almost constant ($\sim$1). Thus, feedback in submillimetre galaxies is nearly balanced by the self-gravity at $t/t_0 \gtrsim 1$. This means that the starburst activity in submillimetre galaxies could cease at almost any starburst age. As a non-negligible fraction of submillimetre galaxies are found to be old ($t/t_0 \gtrsim 5$), there should be physical mechanisms to supply cold gas into starburst regions and maintain star formation even with such strong feedback. Note that if the star formation in submillimetre galaxies completely ceases at $t/t_0 \leqslant 2$, the present-day colours of submillimetre galaxies could not be as red as massive elliptical galaxies.

When submillimetre galaxies reside in a large-scale gravitational potential well, probably due to dark matter, the star formation activity would not completely cease, as the gas can easily fall back to starburst regions again. Recently, a strong clustering feature of submillimetre galaxies was tentatively detected (Blain et al. 2004). This implies that submillimetre galaxies could actually reside in the densest regions in the Universe. Also note that the presence of the massive dark halo is necessary to explain the surface brightness profile at X-ray wavelengths from nearby elliptical galaxies (e.g. Trinchieri, Fabbiano & Canizares 1986; Matsushita et al. 1998). If this is the case, the mixing of gas could occur in the scale of a dark halo, i.e. the chemical evolution in multiple starburst regions may be related to each other. Also, the dark halo would ensure the merging process of multiple starburst regions.

In summary, we suggest that massive submillimetre galaxies consist of multiple self-regulated starbursts in the dark halo. In such systems, how the starburst activity ceases is determined not by the feedback from the starburst, but by the depth of the gravitational

potential of the dark halo. This means that both the resulting stellar mass and the stellar metallicity are controlled by one physical parameter, i.e. the gravitational potential of the dark halo. This ensures the metallicity–mass relation for elliptical galaxies. Therefore, the presence of the massive dark halo may be important to explain the tightness of the CM relation for elliptical galaxies.

6 CONCLUSIONS

We analyse submillimetre galaxies, including EROs and host galaxies of GRBs, using the evolutionary SED model of starburst galaxies. This model allows us to investigate the intrinsic properties of submillimetre galaxies as starbursts. We determine the evolutionary phase of submillimetre galaxies, and derive the stellar mass and metallicity. Then, we predict the colour, magnitude and size of present-day descendants of submillimetre galaxies, based on the results of the SED fitting. This prediction is more reliable for old submillimetre galaxies ($t/t_0 \gtrsim 2$), as a large fraction of the gas would have been already used to form stars, and therefore the effect of star formation after the observed epoch is not significant.

We derive the present-day scaling relations of submillimetre galaxies, i.e. the colour–magnitude and the size–magnitude relations at $z = 0$. These scaling relations can provide new clues on the evolutionary link between submillimetre galaxies and elliptical galaxies. By comparing them with the observed scaling relations of elliptical galaxies, we have reached the following conclusions.

(i) The predicted present-day colours and magnitudes of submillimetre galaxies suggest that the IMF of submillimetre galaxies is flatter than $\mathrm{IMF}_{1.35}$; otherwise the present-day magnitude of submillimetre galaxies become brighter than the brightest elliptical galaxies.

(ii) With $\mathrm{IMF}_{1.10}$, the predicted colours and magnitudes of old submillimetre galaxies are consistent with the observed CM relation of elliptical galaxies. The mean present-day magnitude of submillimetre galaxies is similar to that of L^* elliptical galaxies. This implies that these submillimetre galaxies are quite likely to evolve into present-day elliptical galaxies after the starburst event.

(iii) The derived effective radii of less massive submillimetre galaxies ($M_B \sim -19$ mag at $z = 0$) are consistent with the observed size–magnitude relation of elliptical galaxies. The small size of massive submillimetre galaxies, compared with the size of ellipticals with a similar mass, suggests that they consist of multiple starburst regions. When the multiplicity of starburst regions is taken into account, the resulting effective radii become consistent with observations (within the uncertainty).

Furthermore, we find that starbursts in submillimetre galaxies are self-regulated, i.e. feedback is nearly balanced by the self-gravity. This mechanism may be important for explaining the tightness of the colour–magnitude relation for elliptical galaxies.

ACKNOWLEDGMENTS

TT would like to thank to N. Shibazaki, V. Vansevičius, T. Matsumoto, M. Rowan-Robinson and G. White for their encouraging support. We are grateful to the referee S.C. Chapman for providing valuable data and sensible comments that significantly improved the quality of the paper. This work was financially supported in part by a Grant-in-Aid for Scientific Research (nos 11640230, 13011201, 13640230 and 14540220) by the Japanese Ministry of Education, Culture, Sports and Science. This research has been supported in part by a Grant-in-Aid for Centre-of-Excellence (COE) research. Also, TT acknowledges the support of PPARC.

REFERENCES

Afonso J., Mobasher B., Chan B., Cram L., 2001, ApJ, 559, L101
Alexander D. M. et al., 2003, AJ, 125, 383
Arimoto N., Yoshii Y., 1986, A&A, 164, 260
Arimoto N., Yoshii Y., Takahara F., 1992, A&A, 253, 21
Baugh C. M., Cole S., Frenk C. S., 1996, MNRAS, 282, 27
Bautz M. W., Malm M. R., Baganoff F. K., Ricker G. R., Canizares C. R., Brandt W. N., Hornschemeier A. E., Garmire G. P., 2000, ApJ, 543, L119
Bender R., Burstein D., Faber S. M., 1992, ApJ, 399, 462
Benson A. J., Frenk C. S., Baugh C. M., Cole S., Lacey C. G., 2001, MNRAS, 327, 1041
Berger E., Diercks A., Frail D. A., Kulkarni S. R., Bloom J. S., Sari R., Halpern J., Mirabal N., 2001, ApJ, 556, 556
Berger E., Cowie L. L., Kulkarni S. R., Frail D. A., Aussel H., Barger A. J., 2003, ApJ, 588, 99
Binney J., 2004, MNRAS, 347, 1093
Blain A. W., Chapman S. C., Smail I., Ivison R., 2004, ApJ, 611, 725
Bower R. G., Lucy J. R., Ellis R. S., 1992, MNRAS, 254, 601
Bower R. G. et al., 2004, MNRAS, 351, 63
Chapman S. C., Smail I., Ivison R. J., Blain A. W., 2002, MNRAS, 335, L17
Chapman S. C., Blain A. W., Ivison R. J., Smail I. R., 2003a, Nat, 422, 695
Chapman S. C., Windhorst R., Odewahn S., Conselice H. Y. C., 2003b, ApJ, 599, 92
Chapman S. C., Scott D., Windhorst R. A., Frayer D. T., Borys C., Lewis G. F., Ivison R. J., 2004, ApJ, 606, 85
Clements D. L. et al., 2004, MNRAS, 351, 447
Cole S., Lacey C. G., Baugh C. M., Frenk C. S., 2000, MNRAS, 319, 168
Combes F., Boissé P., Mazure A., Blanchard A., 1995, in Galaxies and Cosmology. Springer-Verlag, Berlin, p. 96 (translated by M. Seymour)
Dey A., Graham J. R., Ivison R. J., Smail I., Wright G. S., Liu M. C., 1999, ApJ, 519, 610
Diaferio A., Kauffmann G., Balogh M. L., White S. D. M., Schade D., Elligson E., 2001, MNRAS, 323, 999
Djorgovski S., Davis M., 1987, ApJ, 313, 59
Downes D., Solomon P. M., 2003, ApJ, 582, 37
Dressler A., Lynden-Bell D., Burstein D., Davies R. L., Faber S. M., Terlevich R., Wegner G., 1987, ApJ, 313, 42
Dunlop J. S. et al., 2004, MNRAS, 350, 769
Eales S., Lilly S., Gear W., Dunne L., Bond J. R., Hammer F., Le Fevre O., Crampton D., 1999, ApJ, 515, 518
Elbaz D., Flores H., Chanial P., Mirabel I. F., Sanders D., Duc P.-A., Cesarsky C. J., Aussel H., 2002, A&A, 381, L1
Fabian A. C. et al., 2000, MNRAS, 315, L8
Flores H. et al., 1999a, A&A, 343, 389
Flores H. et al., 1999b, ApJ, 517, 148
Fox M. J. et al., 2002, MNRAS, 331, 819
Frail D. A. et al., 2002, ApJ, 565, 829
Frayer D. T., Ivison R. J., Scoville N., Evans A. S., Yun M., Smail I., Blain A. W., Kneib J.-P., 1998, ApJ, 506, L7
Frayer D. T. et al., 1999, ApJ, 514, L13
Gear W. K., Lilly S. J., Stevens J. A., Clements D. L., Webb T. M., Eales S. A., Dunne L., 2000, MNRAS, 316, L51
Genzel R., Baker A. J., Tacconi L. J., Lutz D., Cox P., Guilloteau S., Omont A., 2003, ApJ, 584, 633
Georgakakis A., Mobasher B., Cram L., Hopkins A., Lidman C., Rowan-Robinson M., 1999, MNRAS, 306, 708
Hughes D. H. et al., 1998, Nat, 394, 241
Ivison R. J., Smail I., Le Borgne J.-F., Blain A. W., Kneib J.-P., Bezecourt J., Kerr T. H., Davies J. K., 1998, MNRAS, 298, 583

Ivison R. J., Smail I., Frayer D. T., Kneib J.-P., Blain A. W., 2001, ApJ, 561, L45
Ivison R. J. et al., 2002, MNRAS, 337, 1
Kauffmann G., Charlot S., White S. D. M., 1996, MNRAS, 283, L117
Keel W. C., Wu W., Waddington I., Windhorst R. A., Pascarelle S. M., 2002, AJ, 123, 3041
Kodama T., Arimoto N., 1997, A&A, 320, 41
Kodama T., Arimoto N., Barger A. J., Aragon-Salamanca A., 1998, A&A, 334, 99
Lilly S. J., Eales S. A., Gear W. K., Hammer F., Le Fevre O., Crampton D., Bond J. R., Dunne L., 1999, ApJ, 518, 641
Marinoni C., Monaco P., Giuricin G., Costantini B., 1999, ApJ, 521, 50
Massey P., Johnson K. E., Degioia-Eeastwood K., 1995, ApJ, 454, 151
Matsushita K., Makishima K., Ikebe Y., Rokutanda E., Yamasaki N. Y., Ohashi T., 1998, ApJ, 499, L13
Neri R. et al., 2003, ApJ, 597, 113
Pierre M. et al., 2001, A&A, 372, L45
Piro L. et al., 2002, ApJ, 577, 680
Sato Y., Cowie L. L., Kawara K., Taniguchi Y., Sofue Y., Matsuhara H., Okuda H., 2002, ApJ, 578, L23
Sato Y. et al., 2004, AJ, 127, 1285
Scott S. E. et al., 2002, MNRAS, 331, 817
Serjeant S. et al., 2003, MNRAS, 344, 887
Smail I., Ivison R. J., Blain A. W., 1997, ApJ, 490, L5
Smail I., Ivison R. J., Blain A. W., Kneib J.-P., 2002, MNRAS, 331, 495
Smail I., Ivison R. J., Gilbank D. G., Dunlop J. S., Keel W. C., Motohara K., Stevens J. A., 2003, ApJ, 583, 551
Smith G. P., Treu T., Ellis R., Smail I., Kneib J.-P., Frye B. L., 2001, ApJ, 562, 635
Soucail G., Kneib J. P., Bezecourt J., Metcalfe L., Altieri B., Le Borgne J. F., 1999, A&A, 343, L70
Springel V., White S. D. M., Tormen G., Kauffmann G., 2001, MNRAS, 328, 726
Stanford S. A., Eisenhardt P. R., Dickinson M., 1998, ApJ, 492, 461
Steidel C. C., Adelberger K. L., Shapley A. E., Pettini M., Dickinson M., Giavalisco M., 2000, ApJ, 532, 170
Takagi T., Arimoto N., Hanami H., 2003a, MNRAS, 340, 813 (TAH03)
Takagi T., Vansevičius V., Arimoto N., 2003b, PASJ, 55, 385
Trinchieri G., Fabbiano G., Canizares C. R., 1986, ApJ, 310, 637
Vazdekis A., Arimoto N., 1999, ApJ, 525, 144
Waskett T. J. et al., 2003, MNRAS, 341, 1217
Webb T. M. A., Lilly S. J., Clements D. L., Eales S., Yun M., Brodwin M., Dunne L., Gear W. K., 2003, ApJ, 597, 680
Worthey G., 1994, ApJS, 95, 107
Yoshii Y., Arimoto N., 1987, A&A, 188, 13

APPENDIX A: SUMMARY OF OBSERVATIONS

A1 Extremely red objects

We collect extremely red objects detected at MIR–submillimetre wavelengths. In order to increase the size of the sample, we include EROs detected at MIR wavelengths by *ISO*, although they do not have an observed flux at submillimetre wavelengths. The resulting sample includes HR10, EROJ164023, ISOJ1324-2016 and PDFJ011423.

From the observed spectra, EROJ164023, ISOJ1324-2016 and PDFJ011423 are suggested to be composite starburst–AGN galaxies (Afonso et al. 2001; Pierre et al. 2001; Smith et al. 2001), while there is no signature of AGN in the spectra of HR10 (Dey et al. 1999).

A2 Submillimetre-selected galaxies

A2.1 Canada–UK Deep Submillimetre Survey

The secure optical identifications of six submillimetre sources detected in the Canada–UK Deep Submillimetre Survey (CUDSS) are reported in Lilly et al. (1999), one of which is a nearby spiral galaxy at $z = 0.074$ and therefore excluded in this study. Two submillimetre galaxies (CUDSS 14F and 14A) are associated with radio sources. CUDSS 14F is detected by *ISO* at 6.75 and 15 μm, and therefore this source is most securely identified, despite the faintest submillimetre flux among these sample. Currently, no signature of AGN activity has been found in these submillimetre galaxies (e.g. Gear et al. 2000).

CUDSS14.13 is taken from the new catalogue by Webb et al. (2003). The multiband photometric data are reported in Clements et al. (2003). This source has been detected at X-ray wavelengths (Waskett et al. 2003) and probably contains an AGN.

A2.2 SCUBA 8-mJy survey

The SCUBA 8-mJy survey is the largest submillimetre extragalactic survey undertaken to date, covering 260 arcmin^2. Ivison et al. (2002) performed the optical identification of these submillimetre galaxies in the Lockman Hole and ELAIS N2 regions using the 1.4-GHz imaging map; as a result, 18 out of 30 submillimetre sources are reliably identified as radio sources. The spectroscopic redshift of a few sources are available in Chapman et al. (2003a) and are also provided by S. Chapman (private communication). From this survey, five sources (N2 850.1, N2 850.4, N2 850.8 and LE 850.6) satisfy the requirements for our sample. *R*-band data for LE 850.6 is provided by S. Chapman (private communication).

Although the radio map suggests that N2 850.1 is associated with the bright, compact optical galaxy at $z = 0.845$, Ivison et al. (2002) claim that this galaxy acts as a gravitational lens to amplify the background faint submillimetre source, considering the unreasonable 450-/850-μm and submillimetre/radio spectral indices as a submillimetre source at $z < 1$ (see also Chapman et al. 2002). Assuming that the galaxy at $z = 0.845$ is the true optical counterpart, we fit the SED of this submillimetre source, but found no suitable SED model.

A2.3 Hubble Deep Field and SA13 field

The photometric data and the spectroscopic redshifts of sample in these fields (i.e. SMMJ123600.2+621047, SMMJ123629.13+621045.8, SMM J123607.53+621550.4, SMMJ131212.7+424423 and SMMJ131201.2+424208) are taken from Chapman et al. (2003a) and provided by S. Chapman (private communication).

The deep SCUBA map of HDF is reported by Hughes et al. (1998), which is re-analysed by Serjeant et al. (2003). However, no source is collected from this deep survey, as the detected sources are too faint at submillimetre wavelengths compared with the other sample. Note that even the optical identification of the brightest source HDF850.1 is complicated by the possible gravitational lensing by a foreground galaxy (Dunlop et al. 2004).

A3 Lensed submillimetre galaxies

The effects of gravitational lening have been used to push below the confusion limit of the blank-field surveys. In the list of submillimetre sources by Smail et al. (2002), three submillimetre sources, SMM J02399-0136, SMM J14011+0252 and SMM J02399-0124 have enough photometric data to perform the SED fitting, all of which have spectroscopic redshifts. We adopt lens amplifications of 2.5, 2.8 and 2.5 for SMM J02399-0136, SMM J14011+0252 and SMM J02399-0134, respectively (Smail et al. 2002).

SMM J02399-0136 is one of the brightest submillimetre sources at 850 μm. The optical counterpart of SMM J02399-0136 is a system of two interacting/merging galaxies, named L1 for the compact component and L2 for the disturbed diffuse component. The spectroscopic redshifts ($z = 2.80$) measured for each component suggest that L1 is physically associated with L2. The angular separation between L1 and L2 is approximately 3 arcsec (22 kpc for the adopted cosmology). Each component is resolved by a 1.3-arcsec synthesized beam at 1.4 GHz, and appears to have different radio spectral indices. The UV spectrum of L1 exhibits high-ionization lines with a width of $\sim$1000 km s^{-1} and therefore this component probably has an AGN in the centre. The presence of an AGN is also confirmed by the detection in the hard X-ray range by *Chandra* (Bautz et al. 2000). On the other hand, the presence of a large amount of gas ($\sim 2 \times 10^{11}$ M$_\odot$) is inferred from the strong CO emission lines. This means that a significant fraction of far-infrared (FIR) luminosity could arise from starburst activity. The rest-frame FIR-to-5-GHz flux ratio is similar to that seen in nearby starbursts. These observations suggest that SMM J02399-0136 is a composite starburst–AGN galaxy system.

The optical counterpart of SMM J14011+0252 is an interacting/merging pair of galaxies at $z = 2.56$, J1 and J2 (Ivison et al. 2001). The CO position by Downes & Solomon (2003) differs significantly ($\gtrsim$ 1 arcsec) from those obtained by Frayer et al. (1999) and Ivison et al. (2001); as a result, the new position agrees with the optical position of the J1 complex within the 1σ errors.[3] The high-resolution image with the *HST* shows that the morphology of the J1 component is complex, i.e. the main component with relatively regular shape is associated with an extended envelope. Interestingly, the CO and dust emission are spatially extended over a few arcsec ($\gtrsim$10 kpc). Therefore, this galaxy is powered by starbursts rather than an AGN, which is consistent with the spectral features at a rest frame of of 1200–2400 Å (Ivison et al. 2001). Also, this system is undetected in hard X-ray observations using *Chandra* (Fabian et al. 2000).

SMM J02399-0134 is identified with a ring galaxy at $z = 1.06$, which is also relatively bright at 7 and 15 μm (Soucail et al. 1999). The emission lines [O II] 3727 and [Ne V] 3426 Å are detected, which are typical of starburst galaxies hosting a central AGN (Soucail et al. 1999). The presence of an obscured AGN is confirmed through a detection in the hard X-ray band by *Chandra* (Bautz et al. 2000).

[3]Downes & Solomon (2003) also suggest that SMM J14011+0252 is gravitationally lensed not only by the foreground cluster, but also by an individual galaxy on the line of sight. As this hypothesis has not yet been confirmed well (i.e. the redshift of the suspected lensing galaxy is unknown, individually), we think it is premature to take this effect into account. Therefore, we consider the amplification of the source only by the cluster, and assumed that the J1 complex is the true optical counterpart of SMM J14011+0252.

A4 Submillimetre galaxies in the protocluster region

If submillimetre sources at high redshifts are progenitors of present-day elliptical galaxies, they should be found preferentially in overdensity regions at high redshifts, i.e. in protoclusters.

Smail et al. (2003) report the spectroscopically confirmed, submillimetre-selected companion to a high-z radio galaxy 53W002 which has been shown to reside in an overdensity of Ly-α detected galaxies. Using a 1.4-GHz map, this submillimetre source, SMM J17142+5016, is identified with a narrow-line AGN at $z = 2.390$. This galaxy itself is one of the brightest Ly-α emitters in this region, and associated with an extended (> 6 arcsec) Ly-α halo.

SMMJ221726+0013 is a bright submillimetre galaxy resides in a giant Ly-α halo (Chapman et al. 2004) at $z = 3.098$. This giant Ly-α halo 'blob-1' ($\gtrsim$100 kpc) lies in an overdensity region discovered in the survey of Lyman-break galaxies (Steidel et al. 2000). Chapman et al. (2004) identify the optical counterpart as an elongated galaxy J1. The optical–NIR photometric data of J1 are provided by S. Chapman (private communication). No signature of AGN is found (e.g. Bower et al. 2004; Chapman et al. 2004).

A5 A submillimetre-detected faint 6.7-μm galaxy

The SCUBA observations in the field of a very deep 6.7-μm survey (1σ sensitivity of 3 μJy) with *ISO* result in the detection of three submillimetre sources (Sato et al. 2002). We collect SMMJ131225.7+424350 for which the spectroscopic redshift is available (Sato et al. 2002, 2004).

A6 GRB host galaxies

Recent follow-up observations of GRBs at submillimetre/radio wavelengths indicate that approximately 20 per cent of GRB host galaxies are ULIRGs (Berger et al. 2003). Here we analyse three GRBs with the spectroscopic redshift, i.e. GRB 000210, 000418 and 010222 at $z = 0.846$, 1.119 and 1.477, respectively. All GRB hosts are detected not only at submillimetre, but also at radio wavelengths, and therefore the optical identification is reliable (Frail et al. 2002; Berger et al. 2003).

APPENDIX B: ERROR ESTIMATES OF THE SED FITTING

In Fig. B1, we show contour maps of $\Delta\chi^2$ for the sample used in Section 4, in which $\Delta\chi^2 = 1.0$, 2.71 and 6.63 correspond to probabilities of 68.3, 90 and 99 per cent, respectively, when projected to each axis, i.e. t/t_0 and Θ. In most cases, the contour is elongated along the axis for the starburst age. However, note that the range of the starburst age within the confidence level of 68.3 per cent is reasonably small.

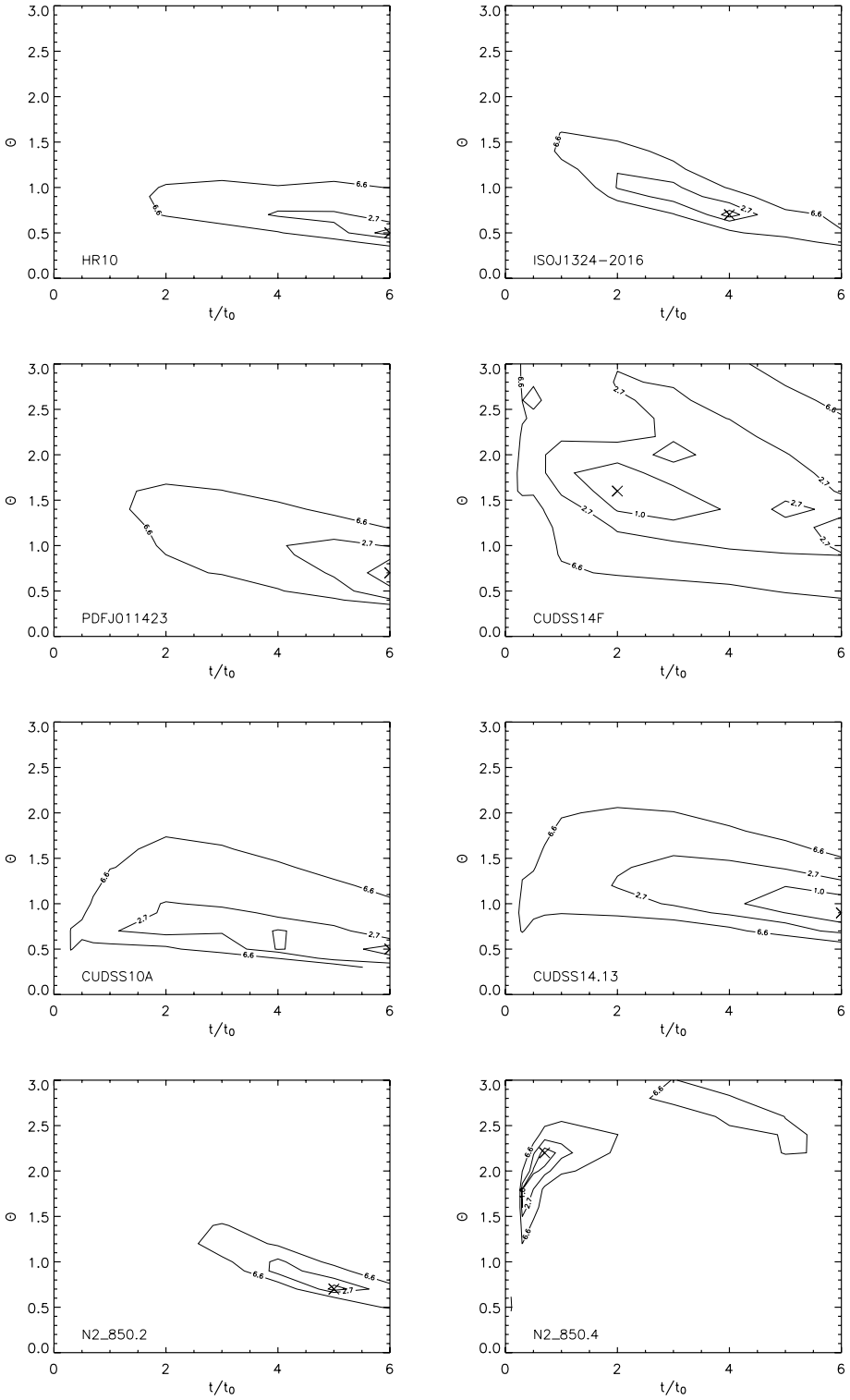

Figure B1. The contour maps of $\Delta\chi^2$ for the sample used in Section 4. The contours are depicted at $\Delta\chi^2 = 1.0$, 2.71 and 6.63, which correspond to probabilities of 68.3, 90 and 99 per cent, respectively (when projected to each axis).

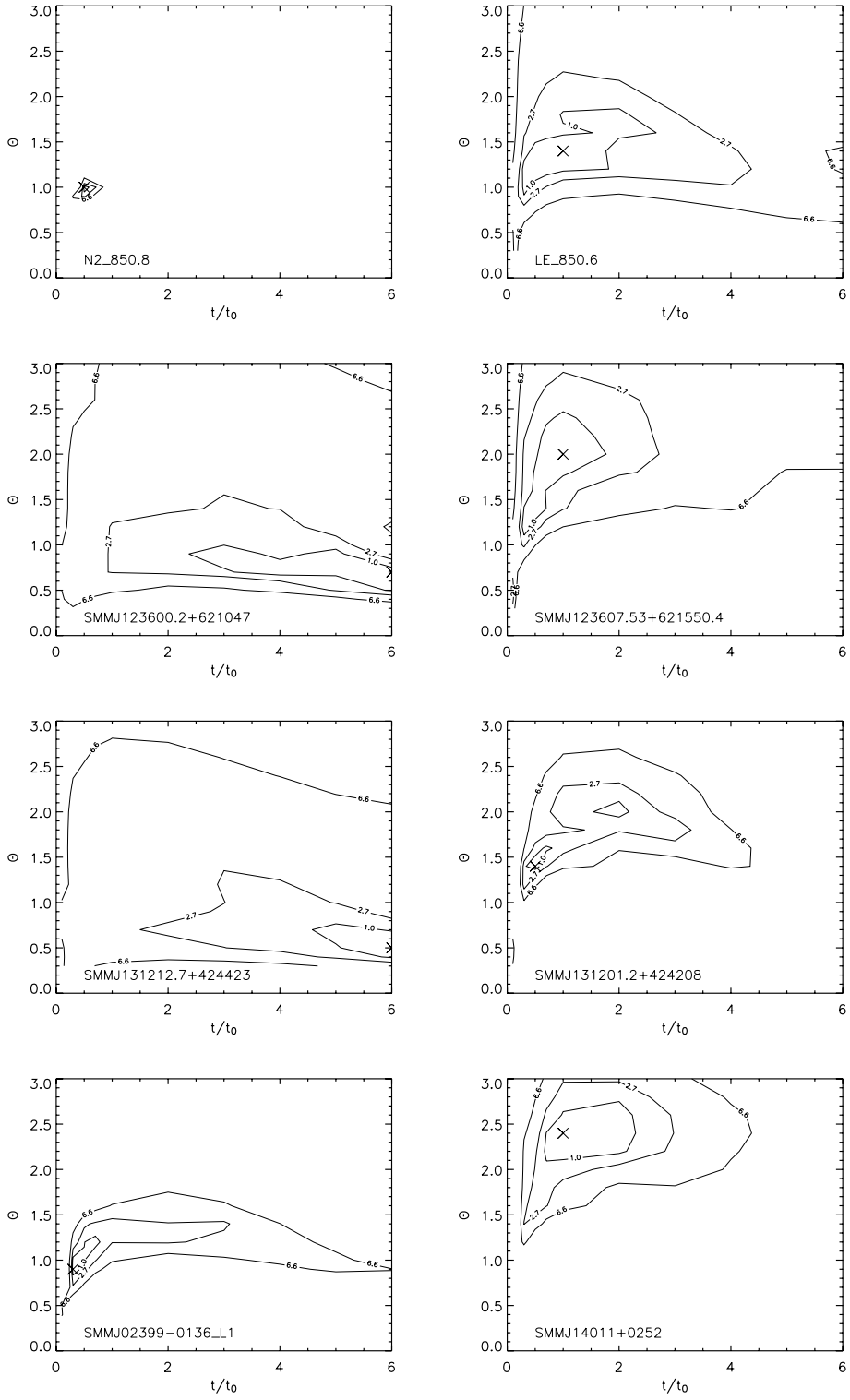

Figure B1 – *continued*

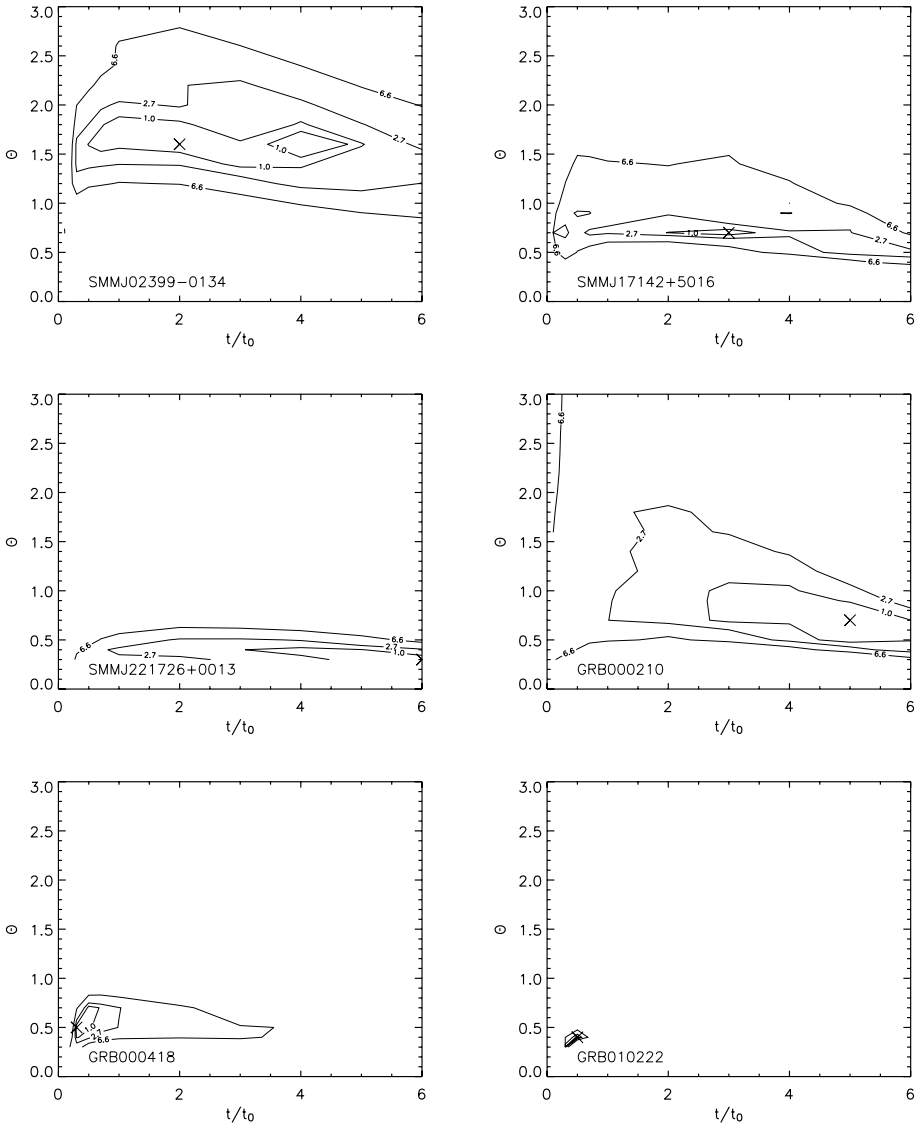

Figure B1 – *continued*

This paper has been typeset from a TEX/LATEX file prepared by the author.